



PAPER • OPEN ACCESS

Serotonin electrochemical detection in tomatoes at MWCNT-AONP nanocomposite modified electrode

To cite this article: Pholoso C Motsaathebe and Omolola E Fayemi 2021 *Mater. Res. Express* **8** 115004

View the [article online](#) for updates and enhancements.

You may also like

- [Development and Application of the Serotonin Voltametric Sensors Based on Molecularly Imprinting Technology](#)
Zhihua Wang, Lijuan Xu, Guofan Wu et al.
- [From reversible to irreversible bistable switches via bifurcations in a gene regulatory network](#)
Lijie Hao, Zhuoqin Yang, Danhong Shen et al.
- [Interference-Free Determination of Dopamine at the Poly\(thionine\)-Modified Glassy Carbon Electrode](#)
A. J. Saleh Ahammad, Narayan Chandra Deb Nath, Guang-Ri Xu et al.

ECS
The
Electrochemical
Society
Advancing solid state &
electrochemical science & technology

DISCOVER
how sustainability
intersects with
electrochemistry & solid
state science research



PAPER

Serotonin electrochemical detection in tomatoes at MWCNT-AONP nanocomposite modified electrode

OPEN ACCESS

RECEIVED

21 September 2021

REVISED

12 October 2021

ACCEPTED FOR PUBLICATION

21 October 2021

PUBLISHED

8 November 2021

Pholoso C Motsaathebe^{1,2} and Omolola E Fayemi^{1,2} ¹ Department of Chemistry, Faculty of Natural and Agricultural Sciences, North-West University (Mafikeng Campus), South Africa² Material Science Innovation and Modelling (MaSIM) Research Focus Area, Faculty of Natural and Agricultural Sciences, North-West University (Mafikeng Campus), South AfricaE-mail: Omolola.Fayemi@nwu.ac.za**Keywords:** serotonin, antimony oxide nanoparticles, multi-walled carbon nanotubes, nanocomposite, electrochemical

Original content from this work may be used under the terms of the [Creative Commons Attribution 4.0 licence](https://creativecommons.org/licenses/by/4.0/).

Any further distribution of this work must maintain attribution to the author(s) and the title of the work, journal citation and DOI.

**Abstract**

This work reports on the successful synthesis of antimony oxide nanoparticles (AONPs) by hydrothermal method, acid treatment of multi-walled carbon nanotubes (f-MWCNTs), and fabrication of a MWCNT-AONP nanocomposite on screen-printed carbon electrodes (SPCE) to detect serotonin (5-HT) in tomatoes. The synthesized nanomaterials were all characterized with x-ray diffraction (XRD) spectroscopy, scanning electron microscopy (SEM), fourier transform infrared (FTIR) spectroscopy, ultraviolet-visible (UV-vis) spectroscopy, and transmission electron microscopy (TEM). The electro-analytic and electrocatalytic experiments were performed utilizing square wave voltammetry (SWV) and cyclic voltammetry (CV) methods. The SPCE-MWCNT-AONP modified electrodes showed better electron transport and improved current response towards detection of 5-HT when compared to other electrodes studied. The current response decreased in this manner, the SPCE-MWCNT-AONP (84.13 μA) > SPCE-fMWCNTs (33.49 μA) > SPCE-AONPs (24.40 μA) > SPCE-bare (2.89 μA). The sensitivity, limit of detection (LoD) and limit of quantification (LoQ) for the SPCE-MWCNT-AONP modified electrode towards 5-HT detection was 0.2863 $\mu\text{A} \mu\text{M}^{-1}$, 24.6 nM, and 74 nM respectively, with linearity from 0.016–0.166 μM ($R^2 = 0.9851$) utilizing SWV. The acquired LoD value for the proposed sensor compared favorably with other chemically modified electrodes from literature. Furthermore, the proposed sensor showed good reproducibility and excellent anti-interference behavior. Real-sample analysis of 5-HT in tomatoes showed excellent recoveries ranging from 91.32 to 108.28%, with an average RSD (%) value of 2.57 ($n = 3$). The obtained results strongly suggest that the proposed novel sensor could be applicable in diagnosing point-of-care diseases and therapeutics.

1. Introduction

Neurotransmitters (NTs) are neurochemicals that aid in neurotransmission between nerve cells; located in the synaptic cells and cell membrane at the axon [1]. The most studied and important class of NTs are catecholamine, which includes dopamine, serotonin, and epinephrine [2]. NTs are involved in many different physiological and biological processes in the human body. NTs regulate stress, rest, feelings, hunger, learning, mood, recollection, attention, and other cognitive functions [3, 4]. However, abnormal levels of NTs in the blood have been linked to neurological diseases and disorders such as depression, stress, bipolar disorder, ADHD, drug addiction, Parkinson's diseases, schizophrenia, and Alzheimer's diseases [5–9]. Therefore, monitoring and evaluation of these biomolecules in the body is of great clinical, pharmaceutical, and medical importance. Since levels of NTs in the body serve as biological markers for various neurological diseases and disorders, a simple, sensitive, selective, low-cost, and quick method of analysis is required. Furthermore, early detection of abnormal NTs levels in the blood leads to early diagnosis of diseases at an early stage and can reduce side effects associated with various diseases, such as memory loss caused by Parkinson's diseases [10].

In the past, NTs were measured with the aid of mass spectroscopy (MS), microdialysis, capillary electrophoresis (CE), and high-pressure liquid chromatography (HPLC) in conjunction with the imaging techniques to improve resolution and ultrasensitive detection [1, 11–13]. These methods proved little success because they were either expensive, time-consuming, slow in response, offered low selectivity, or sensitivity and some are complex to perform. Of recent, electrochemical methods have been gaining popularity amongst researchers towards the detection of NTs. Electrochemical techniques are found to be highly sensitive, simple, time-saving, offer rapid analysis, and increase the sensing ability of NTs inside living entities and *in vivo* real-time analysis [14].

Nonetheless, electrochemical detection of NTs at bare electrodes, such as platinum, gold, and glassy carbon electrodes, presents two main challenges. The challenges arise from the co-existence of NTs with other biomolecules in the body that have similar oxidation potentials called interfering compounds. These interfering compounds cause overlapping oxidation potentials at unmodified electrodes; which reduces the reproducibility and selectivity of the electrode towards detection of NTs in excess interference environment. The second challenge is inferring compounds such as AA and UA at higher concentrations than NTs such as serotonin (5-HT), dopamine (DA), etc. This leads to surface electrode biofouling and affects the LoD of the electrode to detect NTs in an excess interference environment simultaneously. For example, ascorbic acid (AA) is reported to be present at concentrations 100–1000 times higher than that of 5-HT in the blood [15]. To address the issues raised above, many researchers have chosen to utilize nanomaterials including nanoparticles, metal oxide nanoparticles, conducting polymers, metal nanoparticles, inorganic and organic chemicals as electrode modifiers [16]. The nanomaterial mentioned above can be combined to create a nanocomposite with greater electron transfer kinetics and enhanced electrocatalytic properties. Habibi *et al* [17] have shown that modified electrodes significantly increase the electrode's sensitivity and selectivity towards the determination of NTs compared to unmodified electrodes.

Serotonin (5HT) is of significant importance to humans' physiological and biological well-being [18]. 5-HT controls body temperature, mood, ejaculatory tendency, muscular contraction, bowel motility, liver regeneration, bladder control, endocrine regulation, and melancholy, among many other biological activities. However, abnormal serotonin levels in the body have been reported to cause insomnia, migraine, anxiety, blood clotting, and unexpected infant mortality. Moreover, this neurotransmitter has been proven to cause schizophrenia, insomnia, bipolar disorder, and fibromyalgia [5]. Lastly, literature correlates elevated levels of 5-HT in the blood with a dangerous and fatal disease called serotonin syndrome and stimulated cerebral activities.

Due to its medical, chemical, and pharmaceutical importance, traditional methods such as electrochemical (voltammetry) [19], sol-gel [20], capillary electrophoresis (CE) [13], high-pressure liquid chromatography (HPLC) [21], High-pressure liquid chromatography (HPLC) with colorimetry [22], and mass spectrometry (MS) [23] have been carried out to determine 5-HT in excess interfering compound environment using different surface electrode modifiers. From listed techniques, only electrochemical techniques have seen growth in their popularity towards detecting 5-HT in the presence of interfering compounds. The detection of 5-HT in bodily fluids has been accomplished using electrochemical sensors modified with multi-walled carbon nanotubes (MWCNTs), single-walled carbon nanotubes (SWCNTs), nanofibers, graphene, metal nanoparticles, metal oxide nanoparticles, and polymers [24].

The screen-printed electrodes (SPEs) have found new interest amongst researchers because they are inexpensive to mass-produce, disposable, sensitive, portable, easy to use, versatile, reliable, and allow for high reproducibility for *in situ* analysis compared to solid electrodes such as glassy carbon electrodes (GCEs) [24–26]. Another advantage of SPEs over solid electrodes is that they require no polishing on the surface of the electrode [27]. Hence, their wide application in electro-analytical chemistry and environmental, clinical, and agricultural-food areas as electrochemical sensors [28].

Nanotechnology has been instrumental in the development of electrochemical sensors and biosensors. For example, nanotechnology has helped produce small, portable, intelligent sensors requiring little energy to operate. As a result, sensors can be manufactured at a large scale at an economically viable price [29]. Because of their exceptional characteristics, nanoparticles (NPs) have been utilized in electrochemical sensor applications. These characteristics include a high surface area to volume ratio, more active absorption sites, high reactivity, and compact size. Hence, their wide adoption across biomedical, industrial, food and agriculture sectors and environmental analysis [30, 31].

Owing to their tiny crystallite size, semiconductor metal oxide-based nanomaterials have been widely employed as sensors in many applications [32]. Semiconducting metal oxide-based sensors are tiny, durable, affordable, sensitive, and simple to manufacture, making them ideal for handheld portable medical diagnostic devices [32]. Owing to their exceptional chemical stability, real-time monitoring, and ease of manufacturing, they have been utilized to build very sensitive gas sensors [33]. Antimony oxide nanoparticles (AONPs) have exceptional features such as a high refractive index, high resistance to abrasion, high proton conductivity,

outstanding mechanical strength, and high proton absorptive capacity, which underpins their extensive use in the chemical, sensing, and semiconductor fields [31, 34]. In the chemical industry, these nanoparticles are added to rubber, paints, textile, plastic, etc., as flame retardant synergists [35, 36].

Furthermore, they can be incorporated into alloys and still be used as a catalyst in some reactions. For example, Miura *et al* used an antimony oxide nanocomposite to create a humidity sensor [37]. Furthermore, these nanomaterials can be used to sense gases such as methane [38]. As a consequence of their high heat and electrical conductivity properties, these materials have found application in the manufacturing of optical, electronic, and optoelectric devices such as light-emitting diode (LED) and batteries [39], binary glasses [40], solar cells devices [41], anti-friction alloys, and pottery glaze [42].

Carbon nanotubes (CNTs) are widely used in electrochemical sensors, notably multi-walled carbon nanotubes (MWCNTs). This is attributed to their unique electronic nature, enabling ease of electron transfer and mechanical and structural properties [43, 44]. Acid treatment of CNTs helps eliminate end caps, which generates defect sites and attaches oxygen functional group alleged to assist with adsorption and electron transfer [45]. Carbon nanotubes (CNTs)-metal oxide nanoparticles (MONPs) nanocomposites have been extensively used towards the detection of monoamine neurotransmitters [46–49]. Carbon nanomaterials (CNTs, and graphene)-MONPs nanocomposite electrodes are being studied increasingly due to better optical, electrical, and magnetism characteristics as the consequence of synergies between two nanomaterials [50, 51]. In addition, CNTs aid in the catalytic activity of MONPs [50].

The MWCNT-AONP nanocomposite fabricated electrodes have been successfully used to detect various analytes with excellent results. For instance, Hai *et al* [52] fabricated an electrochemical sensor modified with an MWCNT-AONP nanocomposite modified electrode to simultaneously detect cadmium (Cd^{2+}) and lead (Pb^{2+}) ions in water samples. In the same light, Masibi *et al* [53] used AONP-/SWCNT/PANI nanocomposite modified electrode to detect lindane from river water samples. Their modified electrode displayed an LoD of 2.01 nM towards detection of lindane from river water using square wave voltammetry. In another study, Cidem *et al* fabricated an electrochemical detector using MWCNT-AONP nanocomposite with a sensitivity for tramadol (TRA) detection from a pharmaceutical sample and their modified electrode showed a linear range from 0.04 μM –30 μM ($R^2 = 0.9901$) with an LoD value of 9.5 nM using cyclic voltammetry technique [54].

Although much research has been done on the determination of 5-HT with other inferring compounds using modified electrodes [44, 55–59], no literature discusses electrochemical detection of 5-HT using MWCNT-AONP nanocomposite modified electrode. This study, therefore, seeks to use chemical sensors to perform electrochemical detection of 5-HT at MWCNT-AONP nanocomposite modified electrodes. The SPCE-MWCNT-AONP nanocomposite modified electrode demonstrated improved electrocatalytic and electro-oxidation properties towards detecting 5-HT compared to other modified and unmodified electrodes. This was attributed to the high surface area, which facilitated faster electron transfer kinetics that increased the selectivity and sensitivity of the electrode towards the detection of 5-HT in an excess AA environment.

2. Methods and materials

2.1. Chemicals and apparatus

The chemicals listed below were acquired and used as the manufacturers delivered them. Sigma Aldrich (USA) provided antimony trichloride (SbCl_3) (99%), multi-walled carbon nanotubes (MWCNTs) (O.D. \times I.D. \times L 10 nm \pm 1 nm \times 4.5 nm \pm 0.5 nm \times 3– \sim 6 μm) (98%), potassium hexacyanoferrate (III) $\text{K}_3[\text{Fe}(\text{CN})_6]$ (99%), Potassium hexacyanoferrate (IV) $\text{K}_4[\text{Fe}(\text{CN})_6]$ (99%), serotonin hydrochloride powder (\geq 98%), ascorbic acid (99.50%), sodium hydroxide (NaOH) (98%), hydrochloric acid (HCL) (32%), and N, N- dimethylformamide (DMF) ($\text{C}_3\text{H}_7\text{NO}$) (99%). Toluene (C_7H_8) (99%) was acquired from the SAARCHEM Pty Ltd (RSA). Sodium hydrogen orthophosphate (Na_2HPO_4) (99%) and sodium dihydrogen orthophosphate (NaH_2PO_4) (99%) were purchased from Glassworld Pty Ltd. (RSA) and Labchem company (RSA). Phosphate buffered saline (PBS) (pH 7) was prepared with appropriate amounts of Na_2HPO_4 , and NaH_2PO_4 and the pH of the solution was adjusted accordingly using 0.1 M NaOH and 0.1 M HCL. While Nitric acid (HNO_3) (\geq 55%) was obtained from Merck Pty Ltd (RSA). Distilled water was utilized throughout the study to prepare chemicals. Electrochemical studies were done using a portable dropsense kit from Metrohm Pty Ltd. (RSA) containing biopotentiostat 300 ($\mu\text{stat-i}$ 400 s), 910 potentiostat mini, Dropview 8400 software disc, one cable connector (CABSTAT1), boxed connector (DRP-DSX4MM), screen printed carbon electrodes (SPCE), and power adapter. VWR European company, a German manufacturer, supplied Whatman No 1 filter papers (size: 150 mm, particle retention: 5–13 μm).

2.2. Synthesis of AONPs

Antimony oxide nanoparticles (AONPs) were synthesized using the hydrothermal method published by Chen *et al* [60]. To get a transparent solution, approximately 2 mM of antimony trichloride (Sb_2Cl_3) was transferred into 20 ml of toluene solution with rapid stirring. To make a lacteous colloid, 20 ml of distilled water was added to the solution. After that, the mixture was stirred for 15 min, and 6 M of NaOH was added to bring the pH to between 8 and 9. After another 20 min of agitation, the solution was placed into a 100 ml Teflon-lined stainless autoclave for 12 h at 120 °C. The resulting white powder was washed repeatedly with 50% ethanol solution and then evaporated at 60 °C for 6 h.

2.3. Synthesis of f-MWCNTs

The synthesis of functionalized multi-walled carbon nanotubes (f-MWCNTs) was done via the nitric acid treatment method. Approximately 300 ml of 1 M nitric acid was used to dissolve 300 mg of multi-walled carbon nanotubes (designated as raw multiwall carbon nanotube: r-MWCNTS). Then the mixture was sonicated in ice water at 50 °C for 4 h. The mixture was filtered with deionized water until pH 7 was reached. The product was left overnight in an oven to dry [61].

2.4. Characterization of the synthesized nanomaterials

Carry series 300, UV-vis spectrophotometer (Agilent technologies, Waldbronn, Germany), FTIR (Agilent technologies, Cary 600 series, Billerica, MA, USA), XRD (Bruker-AXS, Madison, USA), SEM (JEOL company, Peabody, MA, USA), and TEM (Tecnai G2 spirit FEI, USA) techniques were used to characterize all prepared nanomaterials, AONPs, f-MWCNTs, and MWCNT-AONP nanocomposite.

2.5. Synthesis of the MWCNT-AONP nanocomposite

Approximately 2 mg of functionalized multi-walled carbon nanotubes (f-MWCNTs) and 6 mg of antimony oxide nanoparticles (AONPs) were suspended in a 2 ml N, N- dimethylformamide (DMF) solution. Then, the suspension mixture was agitated at ambient temperature for 48 h. The resultant nanocomposite was dried in an oven at 25 °C for 24 h [53].

2.6. Modification of the screen-printed carbon electrodes

The constructed electrodes were modified using the dried cast method. Roughly 2 mg of each synthesized nanomaterials (AONPs, f-MWCNTs, and MWCNT-AONP nanocomposite) were suspended in 1 ml DMF solution. Each suspension was ultra-sonicated for 30 min at room temperature. Then, 20 μl of each suspended mixture was dropped on the surface of the working electrode (SPCE) with a micropipette, then dried at room temperature to get the modified working electrodes [62].

2.7. The electrocatalytic and electro-analytic experiments

The Dropview 8400 software programme from Metrohm Pty Ltd. (RSA) was used to conduct electrochemical experiments at $25 \pm 1^\circ\text{C}$ using 4 mm diameter screen-printed carbon electrodes (DropSense 110) consisting of the working electrode (A/AgCl), counter electrode, and the reference electrode connected to dropview 8400 910 potentiostat mini. Electrochemical characterization and electrocatalytic experiments at the constructed electrodes (SPCE-bare, SPCE/f-MWCNTs, SPCE-AONPs, and SPCE/MWCNT-AONP) were performed using 5 mM $\text{K}[\text{Fe}(\text{CN})_6]^{3-/4-}$ and 0.1 mM 5-HT dissolved in 0.1 M PBS (pH 7) at the scan rate of 25 mVs^{-1} within -0.2 – 1.0 V potential window period using cyclic voltammetry (CV) technique. Electro-analytic experiments were conducted utilizing square wave voltammetry (SWV) to determine the proposed electrode's sensitivity, selectivity, and limit of detection. The parameters for the SWV method were set at the frequency (10 Hz), potential window ranging from -0.2 – 0.8 V, potential amplitude (0.01 V), Estep (0.01 V) and other parameters were left as they were at zero.

2.8. Real-sample analysis

The capacity of the designed electrode to detect 5-HT in the real analysis was done using fresh tomatoes samples purchased from a local supermarket. The tomatoes were blended using a domestic electric blender. The resultant blend was then filtered using Whatman No 1 filter paper to obtain a clear, colourless tomato extract solution. A fixed volume of the tomatoes extract (1 ml) was added to different volumes of the stock solution to make up to 10 ml of the sample. The experiment was repeated three times using the SWV technique.

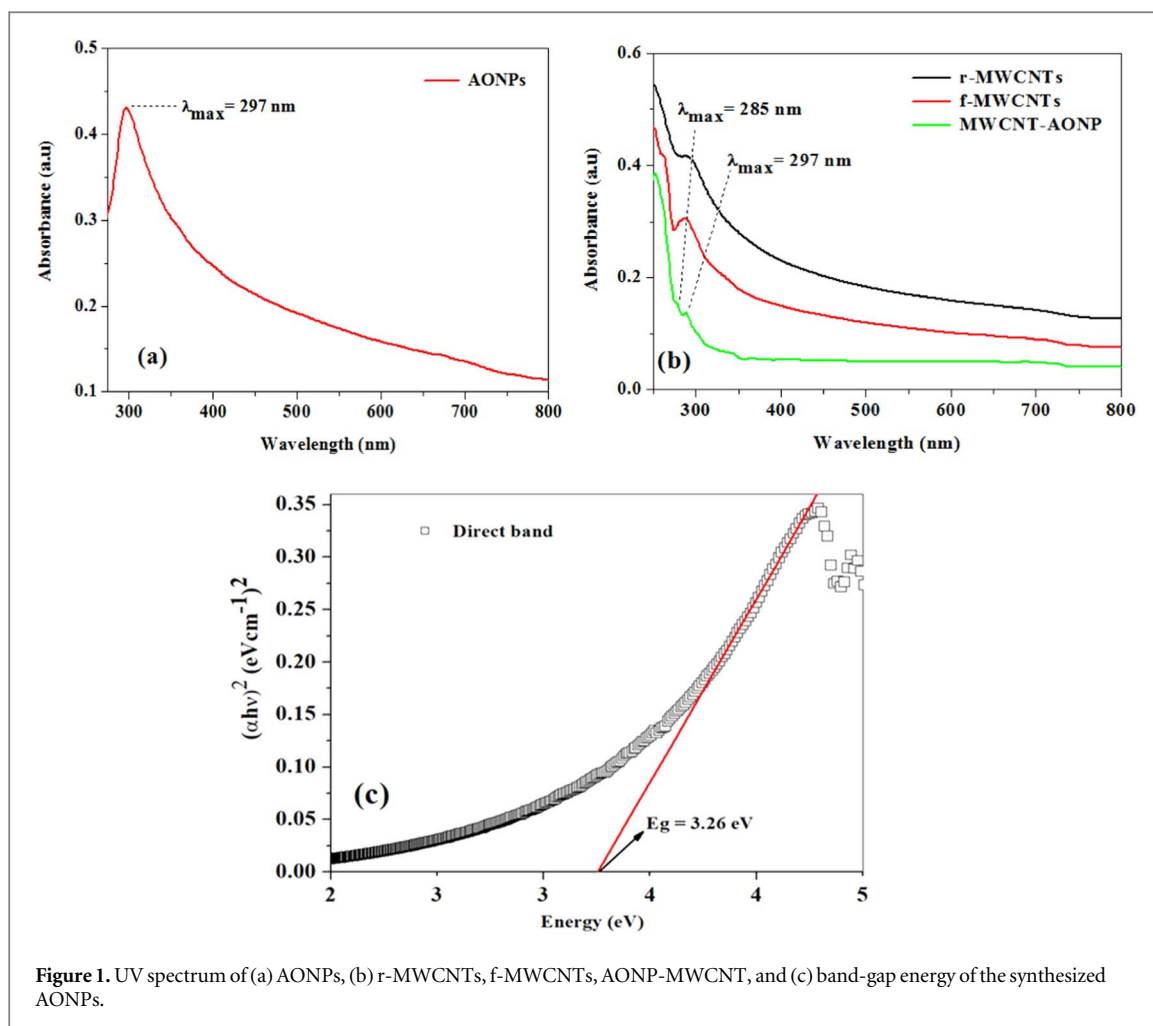


Figure 1. UV spectrum of (a) AONPs, (b) r-MWCNTs, f-MWCNTs, AONP-MWCNT, and (c) band-gap energy of the synthesized AONPs.

3. Results and discussion

3.1. UV–vis characterization of synthesized materials

Figure 1 displays the UV–vis for (a) AONPs, (b) r-MWCNTs, f-MWCNTs, and AONP-MWCNT spectra, and (c) the absorption band energy gap of the synthesized nanoparticles. The spectrum in figure 1(a) indicates the formation of AONPs by an absorption peak at 297 nm [62–64]. A shift to a longer wavelength depends significantly on the particle size and aggregation of the particles [65]. The absence of any absorption peak between 400–800 nm region suggests that the synthesized AONPs can be used to manufacture non-linear optical sensors devices [63, 64]. The direct energy band-gap of AONPs was determined from Tauc's plot shown in figure 1(c). To obtain the direct band energy gap, a straight-line portion of $(\alpha h\nu)$ versus $(h\nu)$ was extrapolated to zero. The direct band-gap energy was 3.26 eV [63]. The spectrum in figure 1(b) shows the UV spectrum of r-MWCNTs, f-MWCNTs, and MWCNT-AONP nanocomposite. From the spectrum, the absorption peaks at 285 nm and 345 nm observed in the AONP-MWCNT nanocomposite were assigned to f-MWCNTs π – π^* transitions [66]. And a peak at 290 nm signifies the presence of AONPs in the AONP-MWCNT nanocomposite.

3.1.2. FTIR characterization of synthesized materials

Figure 2 shows the FTIR bands of (a) AONPs, (b) raw multi-walled carbon nanotubes (r-MWCNTs), functionalized multi-walled carbon nanotubes (f-MWCNTs), and (c) AONP-MWCNT nanocomposite ranging from 450 cm^{-1} – 4000 cm^{-1} regions. Figure 2(a) illustrates the spectrum of f-MWCNTs and r-MWCNTs. The peaks of interest were the absorption bands at 1569 cm^{-1} , 1742 cm^{-1} , 2326 cm^{-1} , 3410 cm^{-1} , and 3780 cm^{-1} which were assigned to the vibrational frequency of carboxylate anion (COO^-), (C=O) of the ($-\text{COOH}$), (O-H) stretching from the $-\text{COOH}$, ($-\text{OH}$) stretching vibrations of the ($-\text{COOH}$), and free hydroxyl group O-H . [61, 67–69]. The presence of these functional groups in the spectra (figure 2(b)) indicated the presence of the ($-\text{COOH}$) on the surface wall of the MWCNTs, which confirmed the successful acid treatment of MWCNTs.

The FTIR bands of AONPs and MWCNT-AONP nanocomposite are represented in figure 2(b). From the spectrum, the characteristics bands of all nanomaterials used to synthesis the nanocomposite are visible. The

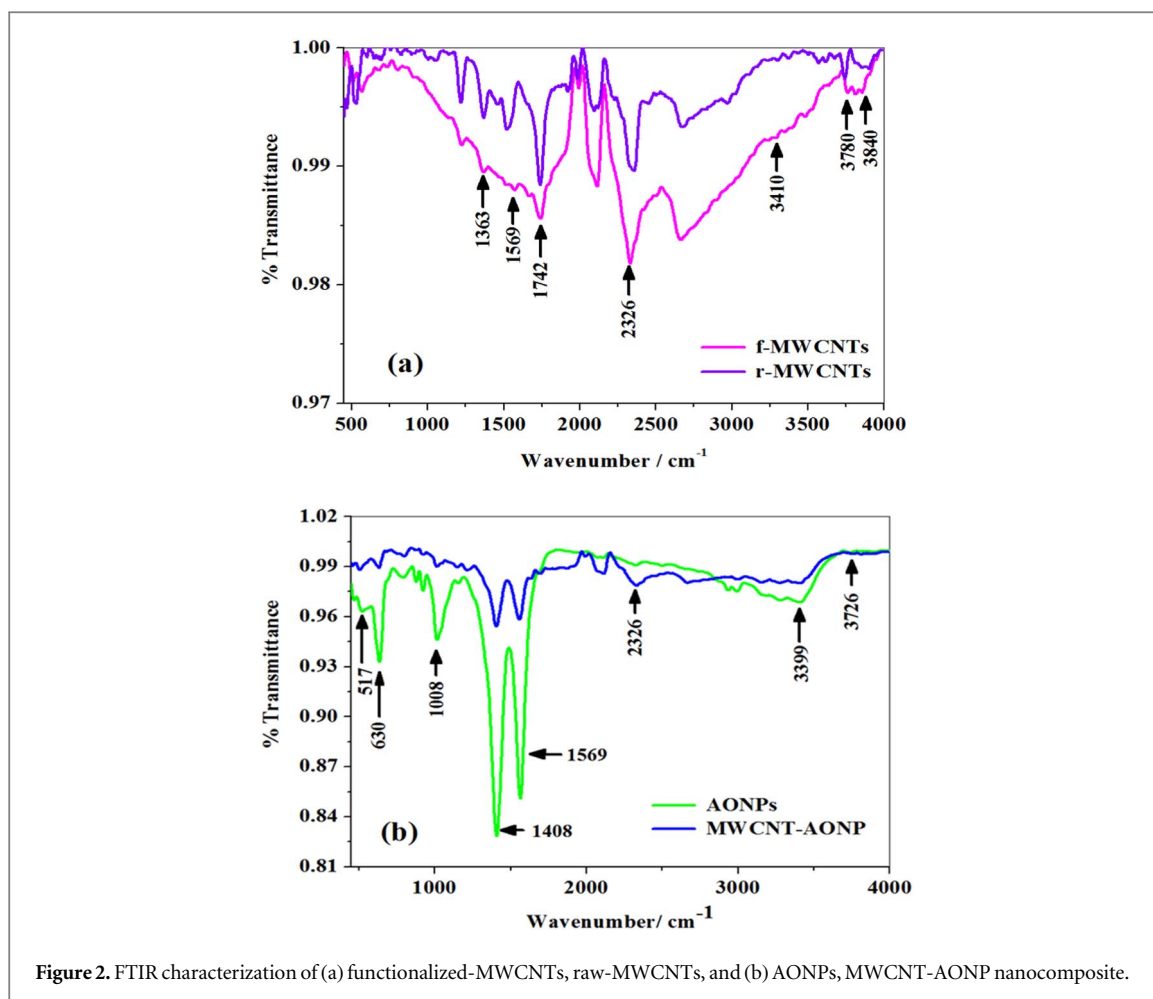


Figure 2. FTIR characterization of (a) functionalized-MWCNTs, raw-MWCNTs, and (b) AONPs, MWCNT-AONP nanocomposite.

absorption band at 517 cm^{-1} , and 630 cm^{-1} indicating the stretching of Sb–O and O–Sb–O of the AONPs, respectively, in the nanocomposite [53, 62–64]. The absorption bands at 3399 cm^{-1} and 37126 cm^{-1} were attributed to the stretching and vibration of (–OH) from the (–COOH), and the bending vibrations of the OH group in water respectively. Absorption bands at 1408 cm^{-1} , 1569 cm^{-1} , and 2326 cm^{-1} indicated the vibrational band of C=C stretching benzenoid rings, (C=O) from the (–COOH) and O–H stretching from (–COOH).

3.1.3. X-ray diffraction of synthesized materials

XRD was utilized to determine the crystallinity and crystal structure of the synthesized AONPs. The XRD patterns of (a) AONPs, (b) fMWCNTs, and (c) MWCNT-AONP nanocomposite are shown in figure 3. The spectrum of AONPs in (figure 3(a)) revealed sharp and intense peaks with no diffraction halo, indicating that the prepared AONPs were of high crystallinity and purity [63]. The peaks at $2\theta = 19.46^\circ$ (110), 25.48° (111), 27.73° (222), 28.46° (121), 33.02° (002), 32.73° (131), 34.84° (012), 36.54° (200), 39.63° (032), 44.33° (042), 46.02° (231), 47.11° (240), 50.47° (161), 55.78° (170), 58.90° (242), and 60.90° (261) corresponds to the formation of AONPs and the formed AONPs showed an orthorhombic phase orientation [60]. Figure 3(b) depicts the XRD of f-MWCNTs. The diffraction peak at $2\theta = 25.94^\circ$ (002) and $2\theta = 50.66^\circ$ (004) corresponded to the amorphous nature of f-MWCNTs [53, 70]. Figure 3(c) represents the XRD image of the MWCNT-AONP nanocomposite showing distinctive diffraction peaks of all nanomaterials used to synthesize the nanocomposite. The presence of AONPs in the MWCNT-AONP nanocomposite is indicated by diffraction peaks at $2\theta = 19.46^\circ$ (110), 27.73° (222), 28.46° (121), 32.73° (131), 33.02° (002), 34.84° (012), 35.90° (200), 44.33° (042), 46.00° (231), 50.47° (161), and 55.78° (170). While the diffraction peak at $2\theta = 25.96^\circ$ (400) indicates the formation of f-MWCNTs in the nanocomposite.

3.2. SEM characterization of synthesized materials

The SEM technique was used to determine the shape of the synthesized nanomaterials and examine the surface area of f-MWCNTs. This is because dry oxidation can cause damages and defects on the surface area of MWCNTs [69]. Shown in figure 4 are the SEM depictions of (a) AONPs, (b) f-MWCNTs, and

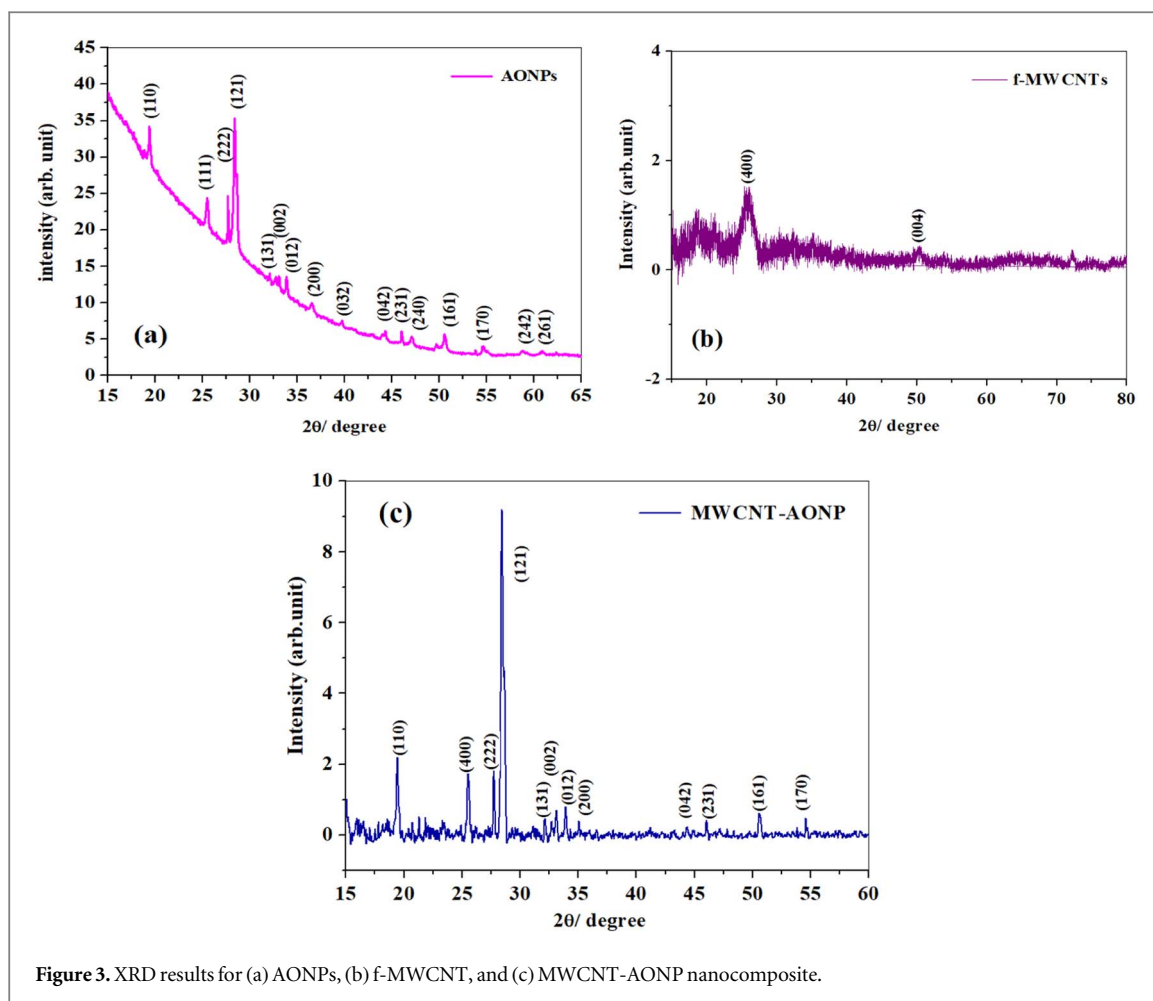


Figure 3. XRD results for (a) AONPs, (b) f-MWCNT, and (c) MWCNT-AONP nanocomposite.

(c) MWCNT-AONP nanocomposite. In figure 4(a), the morphology of synthesized AONPs was evenly distributed rod-like in shape. Figure 4(b) represents the SEM image of f-MWCNTs via the acid treatment method. The morphology of f-MWCNTs was worm-like in shape somewhat similar to this previous study [69]. Moreover, the image showed no signs of any surface damage on the f-MWCNTs surface nor change in their size. SEM depictions in figure 4(c) represent the MWCNT-AONP nanocomposite. The image showed the attachment of AONPs on the surface walls of f-MWCNTs. The presence of AONPs on the surface wall of MWCNTs was taken to mean the successful formation of MWCNT-AONP nanocomposite.

3.2.1. TEM characterization of synthesized materials

TEM is one of the critical microscopic techniques used in science mainly to elucidate the size of the prepared nanomaterials. Depicted in figure 5 are TEM micrographs of (a) AONPs and (b) MWCNT-AONP nanocomposite each at magnifications of 50 nm, and (c) particles size for AONPs. The average particle size for synthesized AONPs was found to be ≈ 25 nm in size while the largest formed nanoparticle reached the size of 95 nm as shown in figure 5(c).

3.3. Cyclic voltammetry comparative study of bare and modified electrodes

Figure 6 represents the comparative cyclic voltammogram for SPCE-bare, SPCE modified with raw MWCNTs (SPCE/raw-MWCNTs), and SPCE modified with functionalized MWCNTs (SPCE/f-MWCNTs) prepared in 5 mM $K[Fe(CN)_6]^{3-/4-}$ redox probe at a scan rate of 25 mVs^{-1} . The peak separations between the SPCE-bare, SPCE/r-MWCNTs, and SPCE/f-MWCNTs were 0.48 V, 0.16 V, and 0.15 V, individually. The peak separations exceeded the anticipated value of 0.059 V predicted for a fast one-electron transfer process for all electrodes. The anodic current peak at SPCE/f-MWCNTs was 1.58 and 2.29 times greater than SPCE/r-MWCNTs and SPCE-bare, respectively. This means that the SPCE/f-MWCNTs electrode is fast at electron transfer and has a greater electro-active surface area than the SPCE and SPCE/r-MWCNTs electrodes.

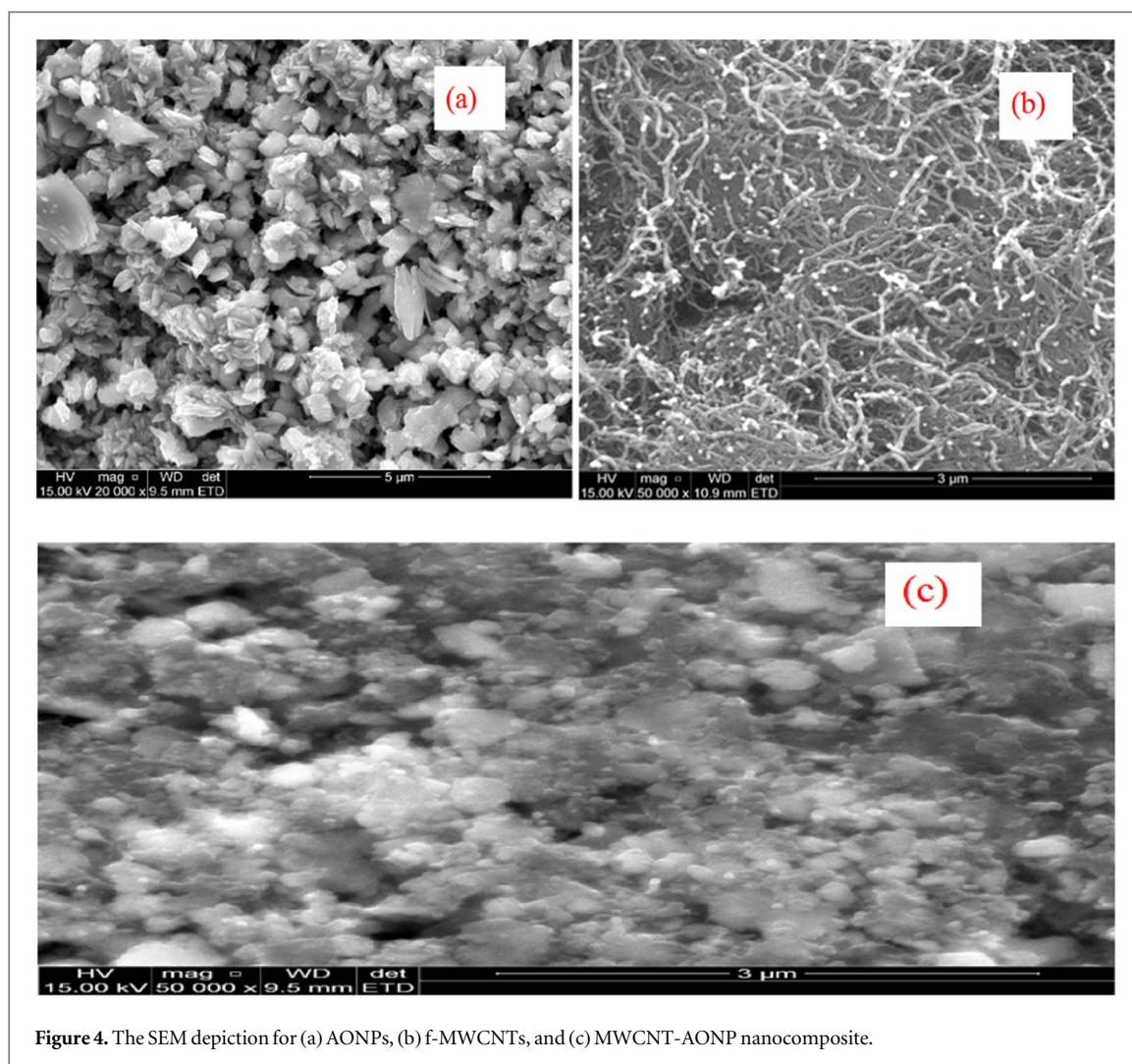


Figure 4. The SEM depiction for (a) AONPs, (b) f-MWCNTs, and (c) MWCNT-AONP nanocomposite.

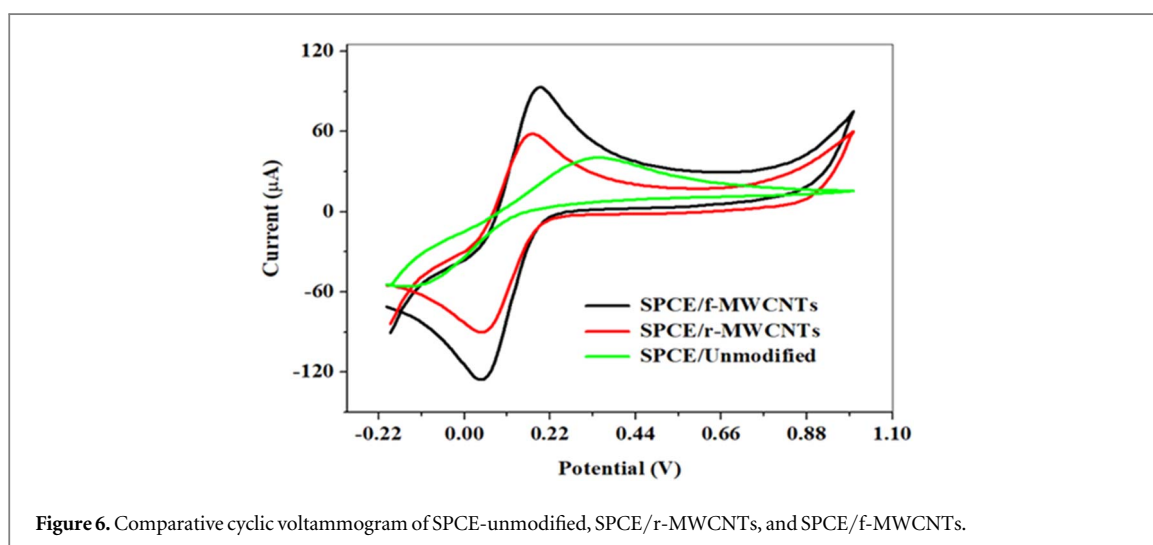
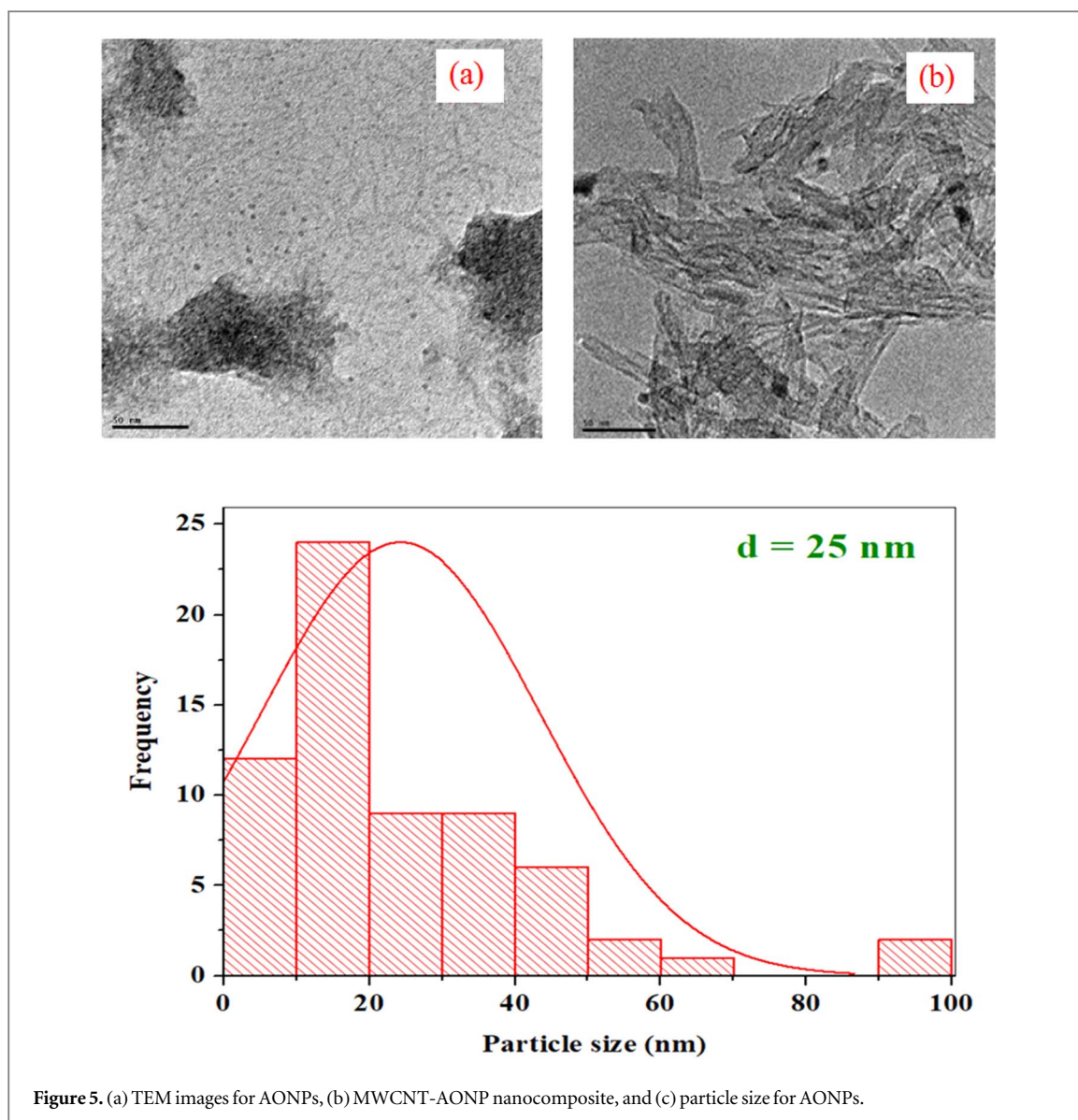
3.4. The effects of pH buffer on the anodic peak of 5-HT

Cyclic voltammograms in figures 7(a) and (c) illustrates the effect of different buffer solution on the anodic peak of 5-HT at the constructed electrode and the inset graphs represent the relationship between anodic peak current versus pH at scan rate (a) 10 mVs^{-1} and (c) 25 mVs^{-1} respectively. This experiment was necessary because NTs such as 5-HT and DA are available in bodily fluid at pH 7.40. The experiment was conducted using 0.1 mM 5-HT made in 0.1 M PBS (pH 3, pH 6, and pH 7, pH 9) solutions at scan rates of 10 mVs^{-1} and 25 mVs^{-1} respectively. In figures 7(a) and (c), an increase in pH resulted in a peak potential shift towards lower values, suggesting the involvement of protons in the reaction for all scan rates. Similarly, insets in figures 7(a) and (c) revealed that as the pH increased, the peak current also increased until pH 7 at which point it rapidly decreased to pH 9 for all scan rates. This suggests that the SPCE- MWCNT-AONP modified electrode was stable at pH 7 PBS. At pH 7, the current response at a scan rate of 25 mVs^{-1} was double that at 10 mVs^{-1} . Due to the significant variation in current responses between the two scan rates, the following experiments were conducted using 0.1 mM 5-HT dissolved in 0.1 M PBS (pH 7) at a scan rate of 25 mVs^{-1} .

The correlation between the peak potential and pH is shown in figures 7(b) and (d), and the relation may be expressed using the following equations: $E_{pa} = 0.034 \text{ pH} + 0.0597$, and $E_{pa} = 0.032 \text{ pH} + 0.58$ with R^2 values of 0.982 and 0.992 for scan rate at 10 mVs^{-1} , and 25 mVs^{-1} respectively. The slopes of dE_p/dpH plots were 0.034 V pH^{-1} and 0.032 V pH^{-1} , closer to the Nernstian theoretical value of 0.059 V pH^{-1} for a one proton per electron stoichiometry for all scan rates. Therefore, The reaction mechanism for 5-HT at the surface of the constructed electrode was a two-protons accompanied by a two-electrons reaction mechanism, as seen in scheme 1 [48, 71].

3.5. Electrocatalytic reduction of 5-HT

Cyclic voltammograms for the SPCE-bare, SPCE-AONPs, SPCE/f-MWCNTs, and SPCE-AONP-MWCNT are shown in figure 8. The voltammograms in figure 8 displayed a distinctive and characteristic shape expected for $5 \text{ mM K} [\text{Fe}(\text{CN})_6]^{3-/4-}$ solution at the scan rate of 25 mVs^{-1} within -0.2 – 1.0 V potential window. The anodic



and cathodic peaks were located at ($I_{pa} = 99.15 \mu\text{A}$; $E_{pa} = 0.22 \text{ V}$), and ($I_{pc} = -124.18 \mu\text{A}$; $E_{pc} = -0.06 \text{ V}$) at SPCE-MWCNT-AONP nanocomposite modified electrode. A shift in the nanocomposite-modified electrode's peak potential towards negative potentials indicates a decrease in the over-potential of the redox

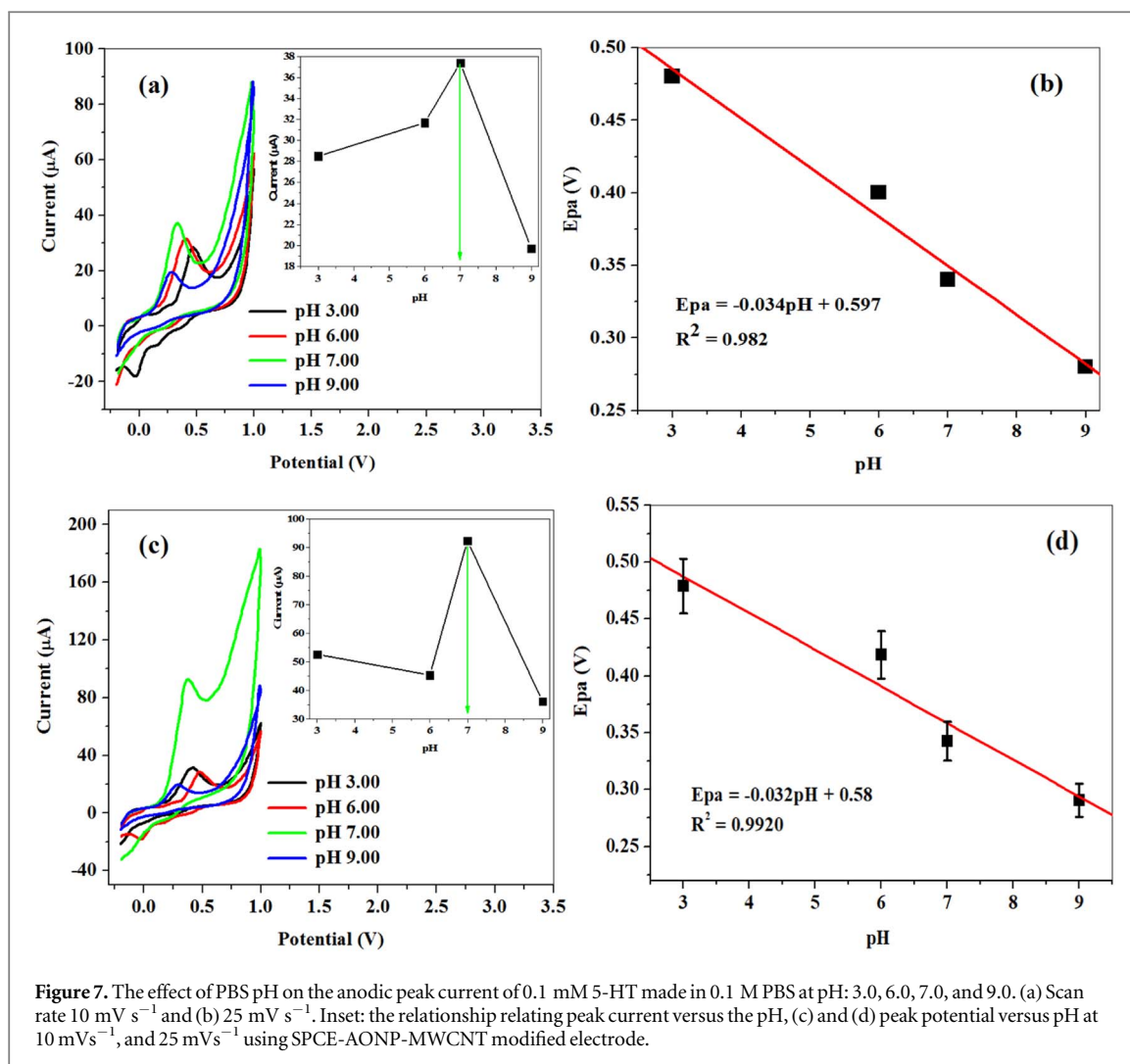
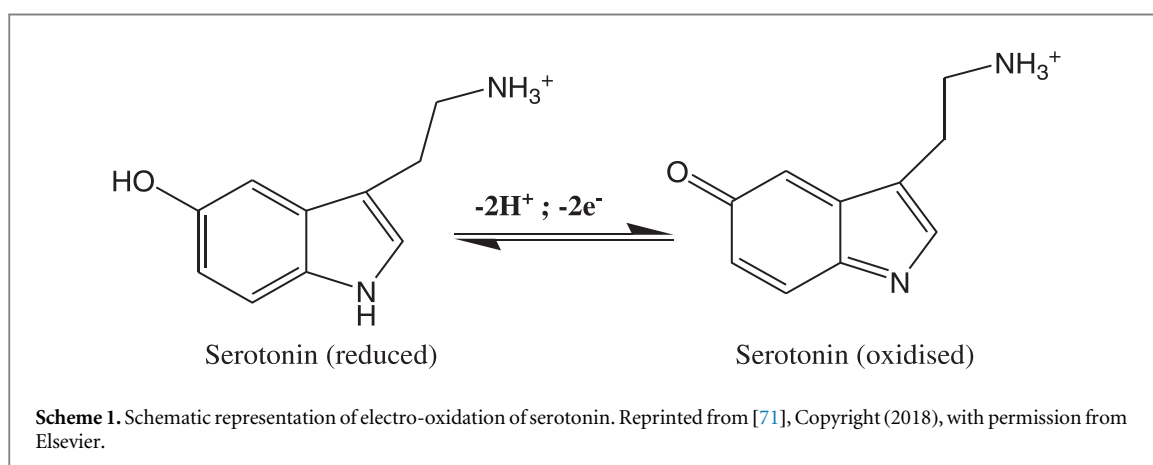


Figure 7. The effect of PBS pH on the anodic peak current of 0.1 mM 5-HT made in 0.1 M PBS at pH: 3.0, 6.0, 7.0, and 9.0. (a) Scan rate 10 mV s⁻¹ and (b) 25 mV s⁻¹. Inset: the relationship relating peak current versus the pH, (c) and (d) peak potential versus pH at 10 mVs⁻¹, and 25 mVs⁻¹ using SPCE-AONP-MWCNT modified electrode.



process at the modified electrode due to enhanced electrocatalytic properties. The voltammogram in figure 8 showed a decrease in current response in the following order, SPCE-MWCNT-AONP > SPCE-fMWCNTs > SPCE-AONPs > SPCE-bare. A higher current response at the nanocomposite modified electrode attests to the synergistic effect between CNTs and AONPs. According to table 1, all electrodes exhibited I_{pa}/I_{pc} values close to one. As a result, all reactions at the surface of modified and unmodified electrodes were reversible. The SPCE-MWCNT-AONP, SPCE-fMWCNTs, SPCE-AONPs, and SPCE-bare, peak to potential separations (ΔE_p) of 0.17, 0.19, 0.21, and 0.48 V were observed. All the peak to potential values for all electrodes were greater than the theoretical value of 0.059 V accepted for a quick-one electron transfer mechanism. Each electrode's resulting active surface area was evaluated using the Randle-Sevcik equation (1). A larger active

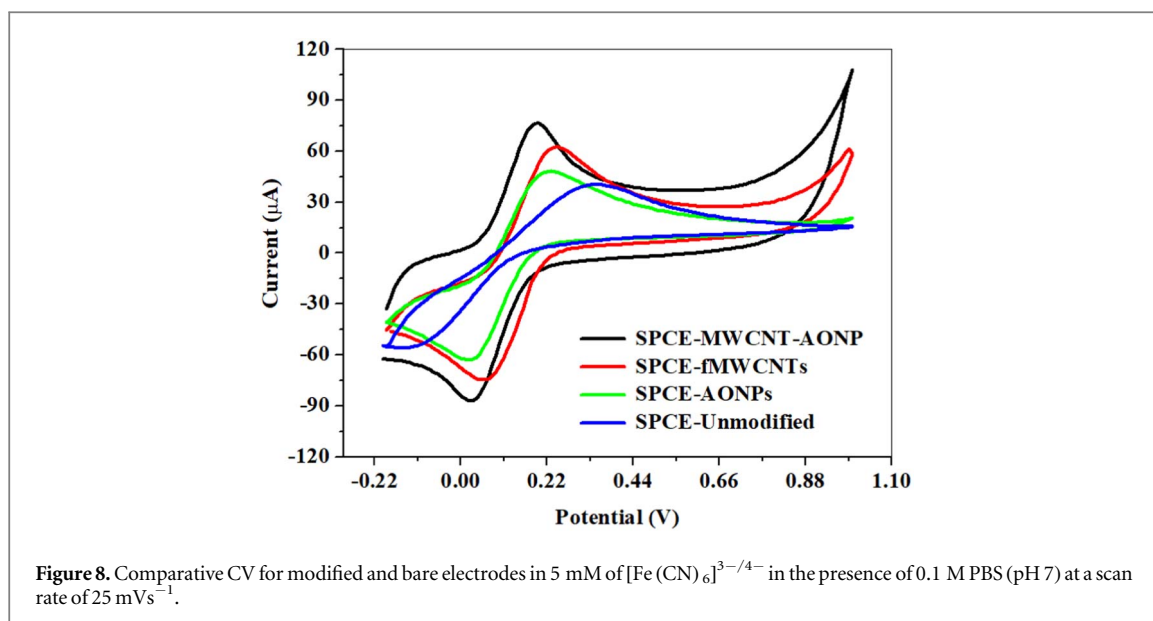


Figure 8. Comparative CV for modified and bare electrodes in 5 mM of $[\text{Fe}(\text{CN})_6]^{3-/4-}$ in the presence of 0.1 M PBS (pH 7) at a scan rate of 25 mVs^{-1} .

Table 1. Summary of CV results for modified and bare electrodes in a 5 mM $[\text{Fe}(\text{CN})_6]^{3-/4-}$ produced in a 0.1 M PBS (pH 7).

Working electrodes	$I_{pa}(\mu\text{A})$	$I_{pc}(\mu\text{A})$	I_{pa}/I_{pc}	$E_{pa}(\text{V})$	$E_{pc}(\text{V})$	$\Delta E_p(\text{V})$	$E^\circ(\text{V})$
Bare SPCE	40.84	-55.82	-0.73	0.35	-0.13	0.48	0.24
SPCE-AONPs	48.17	-64.05	-0.75	0.23	0.02	0.21	0.11
SPCE-f-MWCNTs	65.50	-74.64	-0.88	0.25	0.06	0.19	0.10
SPCE-AONP-MWCNT	76.68	-86.59	-0.89	0.19	0.02	0.17	0.09

surface area indicates increased chances of the electro-active site exposure to an electrocatalytic reaction [72]. The electrodes showed a decrease in active surface area in this manner, the SPCE-MWCNT-AONP (0.716 cm^2) > SPCE-fMWCNTs (0.346 cm^2) > SPCE-AONPs (0.123 cm^2) > SPCE-bare (0.054 cm^2) electrode. The SPCE-MWCNT-AONP modified electrode had thirteen times larger active surface area than the bare electrode. Due to high current response, the SPCE-MWCNT-AONP ($I_{pa} = 76.68 \mu\text{A}$, and $I_{pc} = -86.59 \mu\text{A}$) modified electrode showed a tiny over-potential compared to other modified and bare electrodes. A high over-potential was noted at the bare SPCE with a low current response of $I_{pa} = 40.84 \mu\text{A}$ and $I_{pc} = -55.82 \mu\text{A}$ when compared with the modified electrode. A modified electrode can significantly reduce the electrode's over-potential while increasing the electrode's sensitivity and selectivity for detecting electroactive substances. The above-stated information greatly supports the notion that chemically modified electrodes, especially the SPCE-MWCNT-AONP modified electrodes, exhibit better redox potentials, faster electron transfer kinetics, and stability than unmodified electrode [27]. As a result, the SPCE-MWCNT-AONP modified electrode was selected and used throughout the study.

$$i_p = 2.69 \times 10^5 n^{3/2} A D^{1/2} C v^{1/2} \quad (1)$$

Where i_p , D , C , and $v^{1/2}$ represent the peak currents (Amps), diffusion coefficient (cm^2/s), analyte concentration ($\text{mol}/\text{cm}^{-3}$), and the square root of scan rate (v/mVs^{-1})^{1/2} respectively. Where n and A indicate the number of electrons transported and the active surface area of the modified electrode (cm^2), correspondingly.

3.2. The effects of scan rate on electro-catalysis of 5-HT

Cyclic voltammograms in figure 9(a) show the effect of scan rate study on the anodic peak in 5 mM of $[\text{Fe}(\text{CN})_6]^{3-/4-}$ produced in 0.1 M PBS (pH 7) at scan rates of 10–300 mVs^{-1} . The voltammogram in figure 9(a) showed an anodic peak shifted towards a higher potential and the cathodic peaks shifted towards negative potentials as the scan rate increased, suggesting a diffusion-controlled reaction took place. The reduction and oxidation peak currents increase in proportion to the scan rate, indicating a diffusion-controlled reaction took place as shown in figure (b). Additionally, the voltammogram indicated that an ideal reversible reaction occurred, which is confirmed by the almost identical gradient slopes observed at $I_{pa} = 73.215 \mu\text{A}/(\text{mVs}^{-1})^{1/2} - 133.55$ ($R^2 = 0.993$) and $I_{pc} = -73.549 \mu\text{A}/(\text{mVs}^{-1})^{1/2} + 142.87$ ($R^2 = 0.995$) [73].

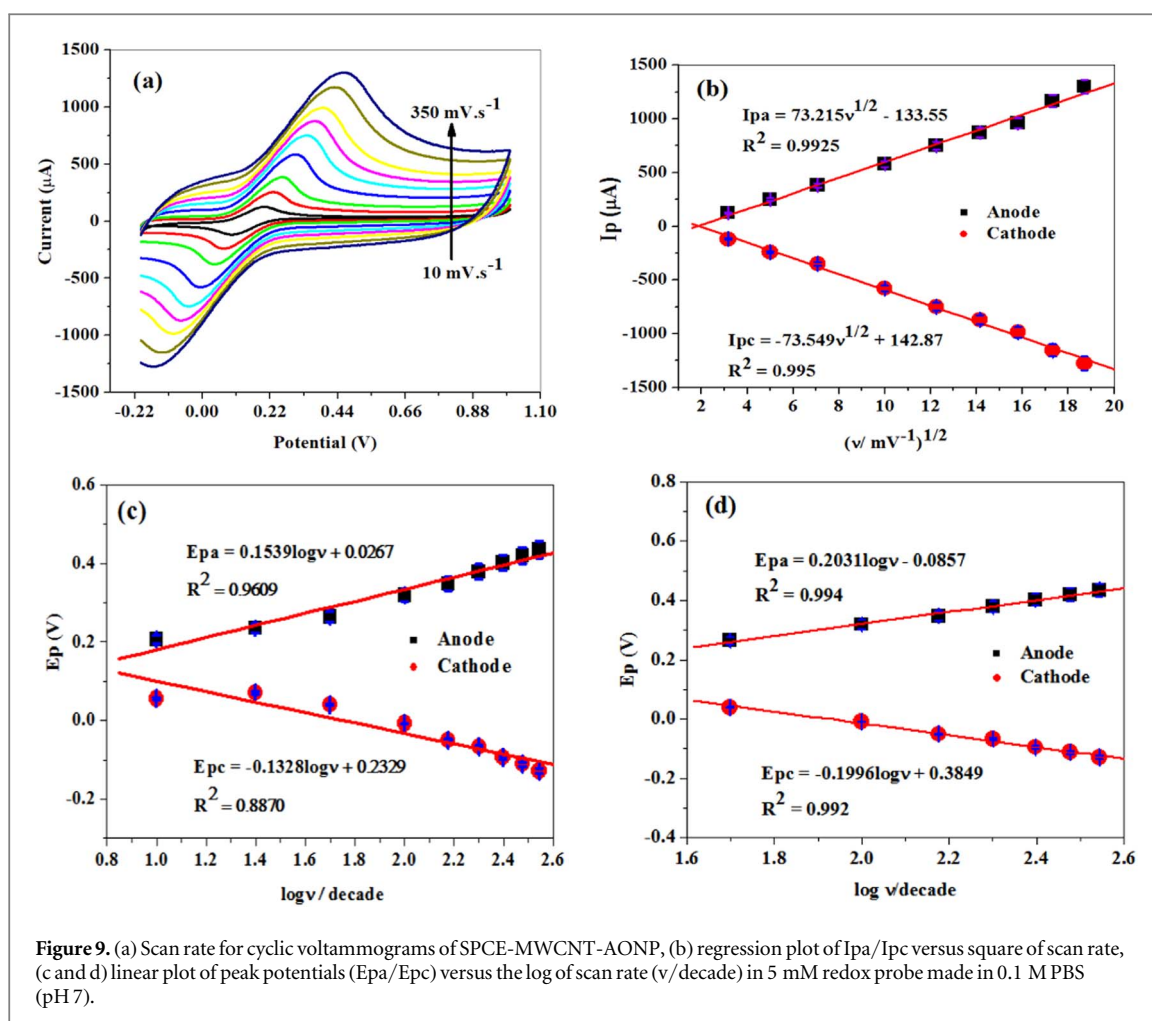


Figure 9. (a) Scan rate for cyclic voltammograms of SPCE-MWCNT-AONP, (b) regression plot of I_{pa}/I_{pc} versus square of scan rate, (c and d) linear plot of peak potentials (E_{pa}/E_{pc}) versus the log of scan rate (v/decade) in 5 mM redox probe made in 0.1 M PBS (pH 7).

The relation between the potential and the scan rate logarithm is shown in figures 9(c) and (d). The Tafel value was determined using a gradient slope of $E_{pa} = 0.2031 \log v - 0.0857$ ($R^2 = 0.994$).

Using the acquired gradient slope, a Tafel value of $406.0 \text{ mV dec}^{-1}$ was determined for the SPCE-MWCNT-AONP modified electrode. The observed Tafel value was greater than the predicted value of 118 mV dec^{-1} , indicating that adsorption or reaction intermediates were involved in the reaction at the surface of the fabricated electrode. The Tafel value was obtained using the Tafel equation (2);

$$E_p = \frac{b}{2} \log v + c \quad (2)$$

Where E_p , b , and c stands for potential, the gradient slope of the graph, and the constant respectively.

The coefficient of electron transfer (α) and the number of electrons transported (n) at the fabricated electrode were determined to be 0.50 and 0.597 ($n = 1$) using equations (3) and (4) assigned as the cathodic and anodic peaks by Laviron [74].

$$\text{Slope} = \frac{-2.3RT}{\alpha nF} \quad (3)$$

$$\text{slope} = \frac{2.3RT}{(1 - \alpha_a)nF} \quad (4)$$

Whereby R , F , T , and α represents the gas constant ($8.314 \text{ J mol}^{-1} \cdot \text{K}$), faradays constant (96500 C), temperature (Kelvins), and the coefficient of electron transport at the fabricated electrode respectively.

The rate constant (k_s) was used to calculate the speed at which the reaction at the SPCE-MWCNT-AONP modified electrode proceeded. For a reversible and quick reaction, the rate constant (k_s) value must be larger than $10^{-2} \text{ cm s}^{-1}$, while for a quasi-reversible and a slow reaction, the rate constant value must be greater than 10^{-4} but less than $10^{-2} \text{ cm s}^{-1}$ [75]. Equation (5) was used to obtain the rate constant value (k_s) of 0.046 cm s^{-1} for the SPCE-MWCNT-AONP modified electrode.

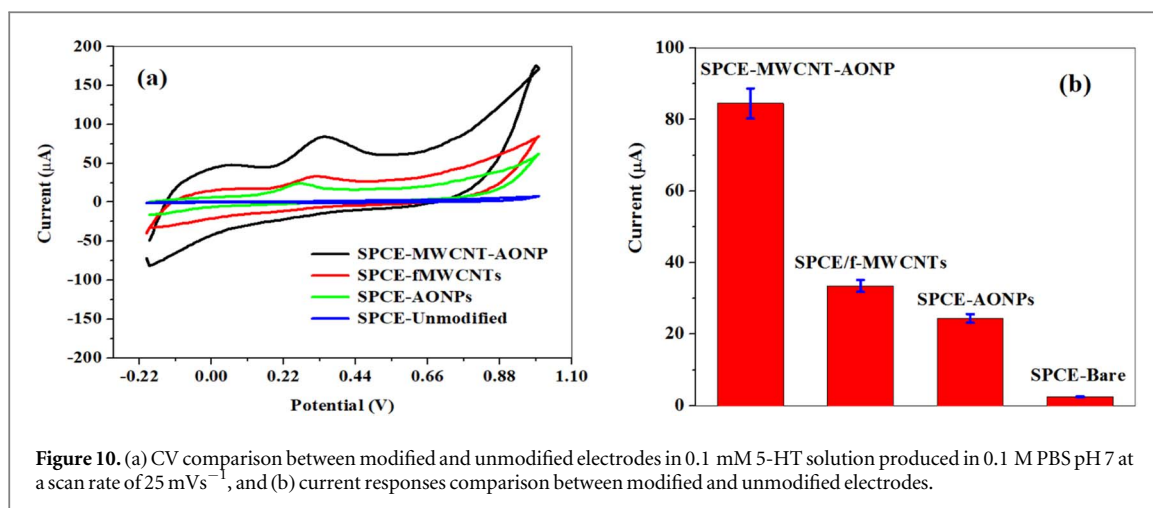


Figure 10. (a) CV comparison between modified and unmodified electrodes in 0.1 mM 5-HT solution produced in 0.1 M PBS pH 7 at a scan rate of 25 mVs⁻¹, and (b) current responses comparison between modified and unmodified electrodes.

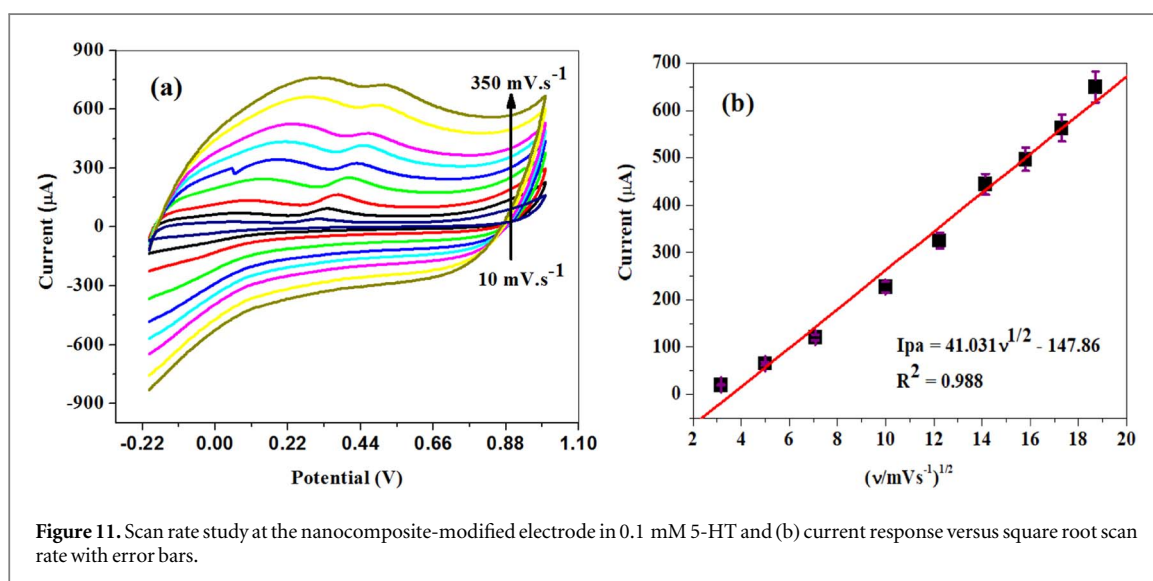


Figure 11. Scan rate study at the nanocomposite-modified electrode in 0.1 mM 5-HT and (b) current response versus square root scan rate with error bars.

$$\log ks = \alpha \log (1 - \alpha) + (1 - \alpha) \log \alpha - \log \frac{RT}{nFv} - \alpha(1 - \alpha) \frac{nFT}{2.3RT} \quad (5)$$

Figure 10 represents the electrochemical oxidation of 0.1 mM 5-HT at various electrodes made in 0.1 M PBS (pH 7) at a scan rate 25 mVs⁻¹. Figure 10(a) displayed a distinctive anodic peak for 5-HT at E_{pa} = 0.35 V for the SPCE-MWCNT-AONP modified electrode. This is in agreement with other works done [48, 57]. Anodic peak potential for SPCE-fMWCNTs, SPCE-AONPs, and SPCE-bare electrodes were located at E_{pa} = 0.32 V, 0.27 V, and 0.50 V respectively. Moreover, the voltammogram showed that the electro-oxidation reaction of 5-HT was irreversible for all electrodes. The SPCE-MWCNT-AONP showed the greatest electrocatalytic response to 5-HT when compared to other modified electrodes. The current response decreased in this manner, the SPCE-MWCNT-AONP (84.13 μA) > SPCE-fMWCNTs (33.49 μA) > SPCE-AONPs (24.40 μA) > SPCE-bare (2.89 μA). The current response at the SPCE-MWCNT-AONP electrode was 29 times greater than at the SPCE-bare. A higher current response to 5-HT observed at the SPCE-MWCNT-AONP modified electrode indicated excellent biocompatibility of the nanocomposite with the analyte and improved electrocatalytic activity. These results show a pattern similar to those obtained in figure 8 using redox probe solution. The linear relationship between scan rate and the anodic peak current is shown in figure 11(a). The voltammogram shows a slight shift in oxidation peak current towards higher potential values with increasing scan rate. Figure 11(b) depicts a linear correlation between the current and square root of scan rate for 5-HT, implying a diffusion-controlled reaction took place.

3.3. Electro-analysis experiment for 5-HT

The proposed sensor's sensitivity and detection limit were carried out using a 0.1 M PBS (pH 7) with various concentrations of 5-HT with the help of SWV. The parameters for the SWV method were set at the frequency (10 Hz), potential window ranging from -0.2–0.8 V, potential amplitude (0.01 V), Estep (0.01 V) and other

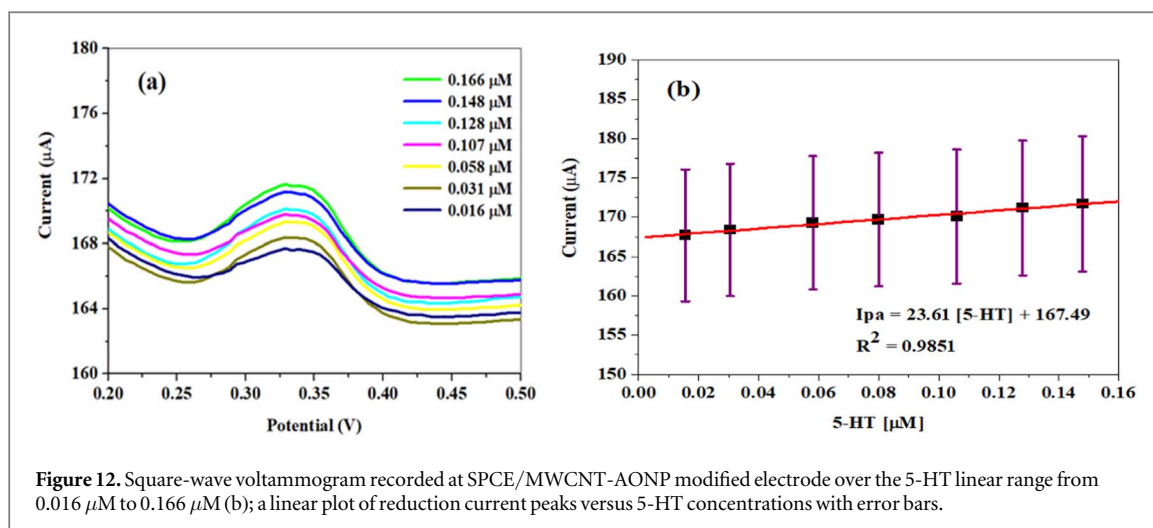


Figure 12. Square-wave voltammogram recorded at SPCE/MWCNT-AONP modified electrode over the 5-HT linear range from 0.016 μM to 0.166 μM (b); a linear plot of reduction current peaks versus 5-HT concentrations with error bars.

Table 2. Comparison with other chemically modified electrodes towards detection of 5-HT.

Modified electrode	Method	Linearity(μM)	Analyte	LOD (μM)	References
Carbon-sphere/GCE	DPV	40–750	5-HT	0.70	[55]
Ionic liquid-DC-CNT/GCE	DPV	5–900	5-HT	2	[76]
CNT-intercalated graphite electrodes	DPV	1–15	5-HT	0.20	[44]
poly-AzrS/MWCNTs/GCE ^a	DPV	0.5–11	5-HT	0.18	[58]
Ach/GCE ^b	DPV	1–30	5-HT	0.50	[77]
COOH-CNT/ME ^c	FSCV	–200.	5-HT	0.07	[78]
CONH ₂ -CNT/ME ^d	FSCV	1–20	5-HT	0.09	[78]
MWCNT-AONP-SPCE	SWV	0.016–0.166	5-HT	0.025	This work

^a poly-AzrS/MWCNTs/GCE = Glassy carbon electrode treated with poly-alizarin red S (AzrS) and MWCNTs.

^b Ach/GCE = Glassy carbon electrode modified with acetylcholine and choline.

^c COOH-CNT/ME = Microelectrodes modified with Carboxylic acid functionalized carbon nanotube.

^d CONH₂-CNT/ME = Microelectrodes fabricated with formamide functionalized carbon nanotube.

parameters were left as they were at zero. The objective was to evaluate and analyze the effect of various analyte concentrations on the current response of 5-HT. Figure 12 displays a directly proportional relationship between the concentration of 5-HT and the current response. The linearity of the SPCE-MWCNT-AONP modified electrode ranged from 0.016–0.166 μM , and a linear regression equation of $I_{pa} = 0.2863 [5\text{-HT}]/\mu\text{A} + 1.6741$ ($R^2 = 0.9851$), and a detection limit (LoD) of 24.6 nM, as displayed in figure 12(b). The obtained data show a strong correlation with this work [54]. The resulting limit of detection (LoD) value was calculated from equation (6), and the limit of quantification (LoQ) for the modified electrode was calculated using equation (7). The LoD and LoQ values were calculated to be 0.025 μM and 74 nM, respectively.

$$\text{LoD} = \frac{3.3 \times \text{SD}}{m} \quad (6)$$

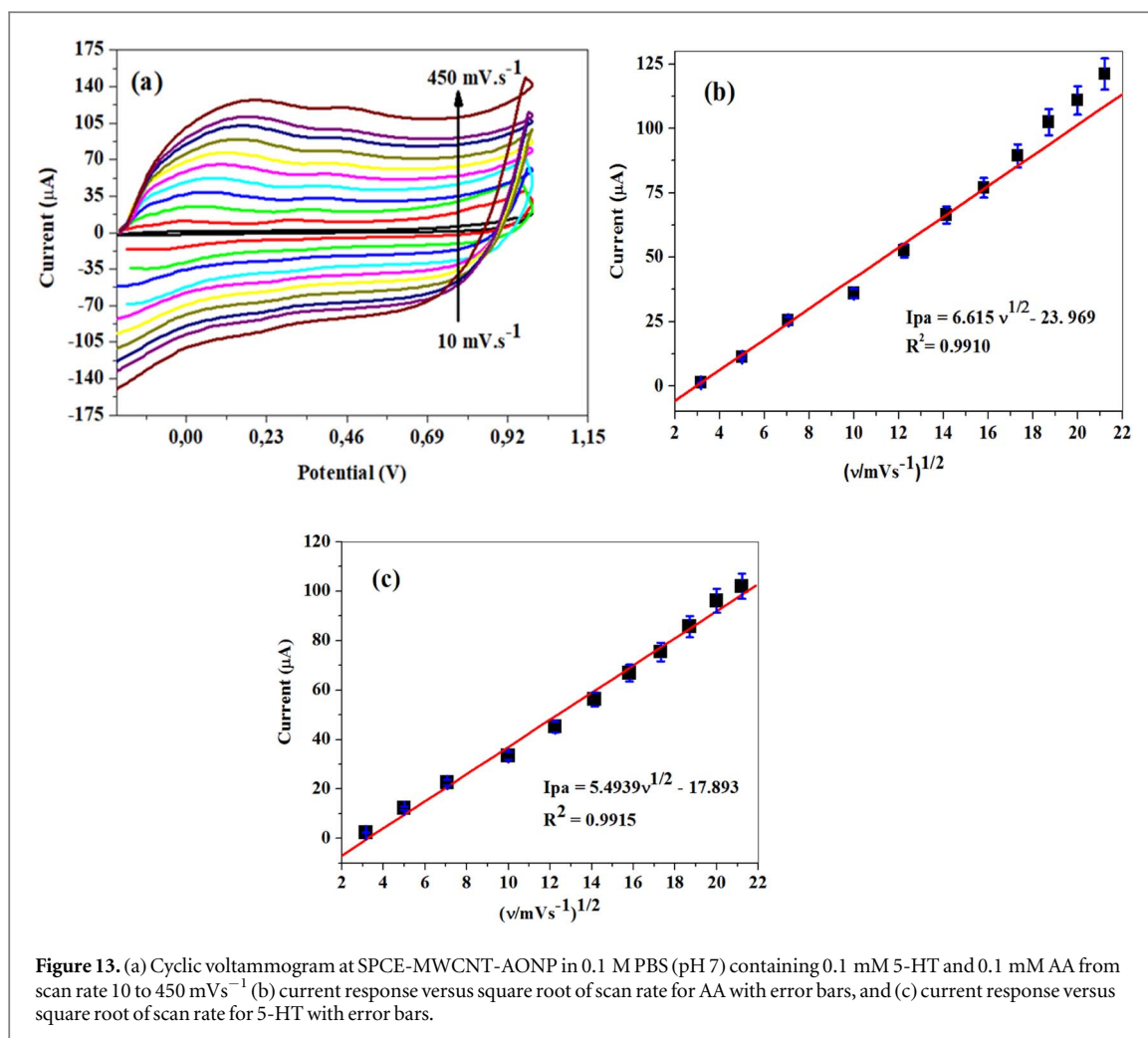
$$\text{LoQ} = \frac{10 \times \text{SD}}{m} \quad (7)$$

SD stands for standard deviation, while m represents the slope of the calibration plot.

As demonstrated in table 2, the obtained results, including the LoD and sensitivity of the SPCE-MWCNT-AONP nanocomposite electrode, compared well to other chemically modified electrodes used to detect 5-HT from literature.

3.4. Selective determination of AA and 5-HT

Cyclic voltammogram was utilized to establish the selective of the proposed electrode by simultaneously detecting 0.1 mM 5-HT and 0.1 mM AA prepared in 0.1 M PBS (pH 7) scan rate ranging from 10–300 mVs^{-1} . Figure 13(a) shows the results of the experiment. An increase in scan rate resulted in a positive peak potential shift for all analytes. However, the electrode showed a higher current response towards AA than 5-HT. At scan rate of 25 mVs^{-1} , AA and 5-HT peak potentials were located at -0.014 V and 0.302 V, respectively. Figures 13(b) and (c) shows the relationship between current response versus square root of scan rate for AA and

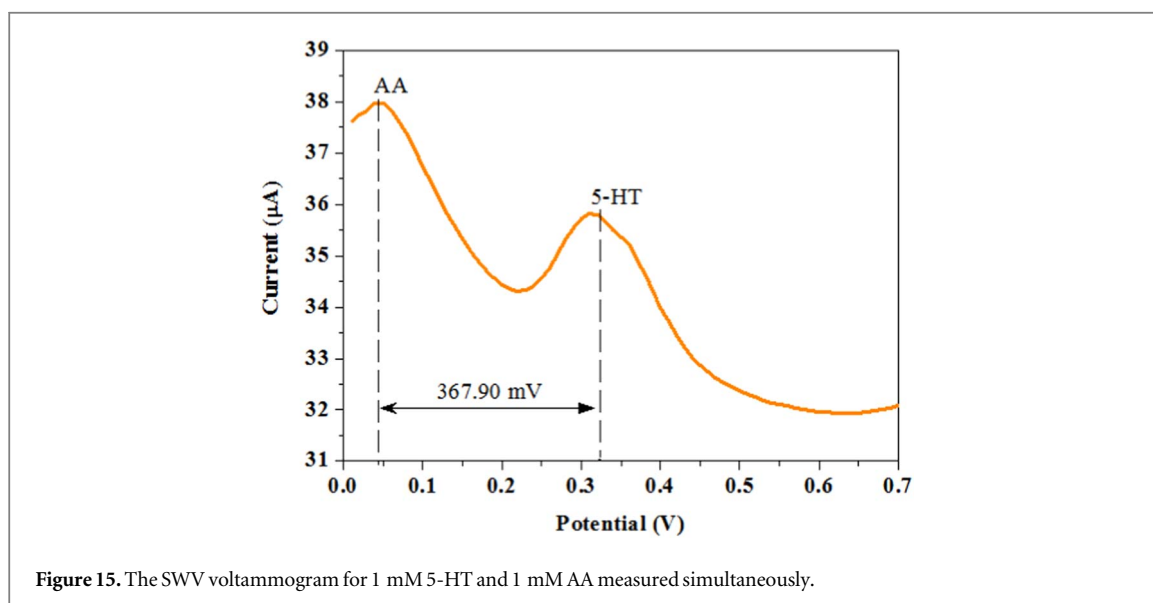
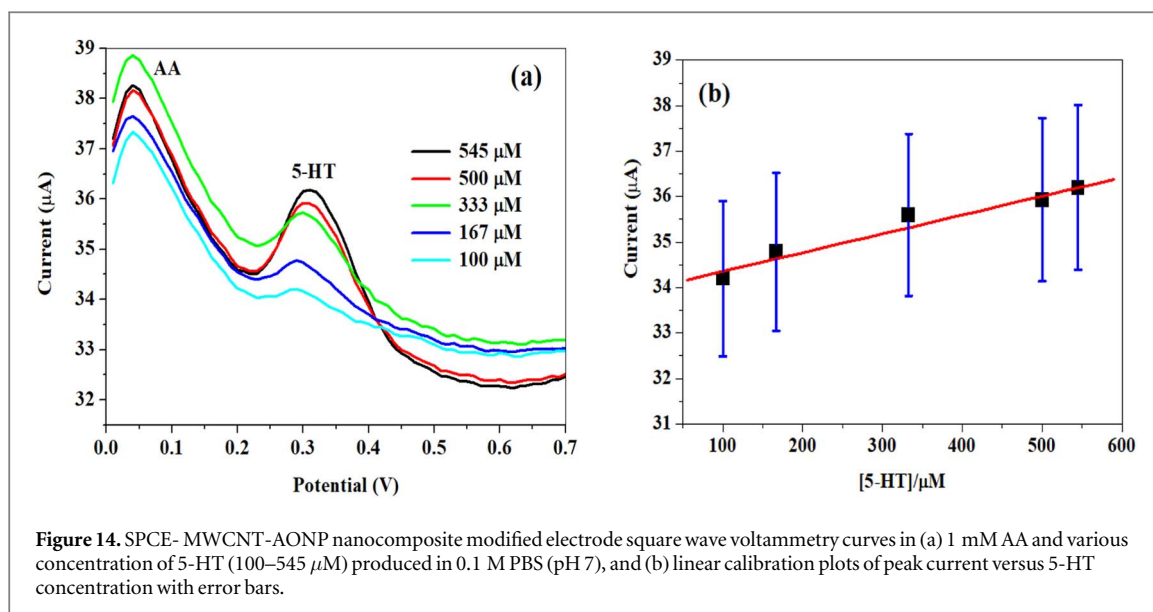


5-HT. A linear relationship between current response and the square root of scan rate for both analytes was observed, suggesting that the reaction at the proposed electrode was diffusion controlled. The linear regression equation for AA and 5-HT were $I_{pa} = 6.615 v^{1/2} - 23.969$ ($R^2 = 0.991$) and $I_{pa} = 5.493 v^{1/2} - 17.893$ ($R^2 = 0.992$). The R^2 value of 5-HT improved significantly compared to those in figure 11.

3.5. Simultaneous detection of 5-HT and AA

The interference study for the proposed electrochemical sensor was done by simultaneously detecting varying concentrations of 5-HT in 1 mM AA solution as an interfering molecule using square wave voltammetry. A higher AA concentration was utilized because interfering compounds such as AA and UA are present in the body fluids at higher concentrations than NTs. From figure 14(a), the peak potentials for AA and 5-HT were located at 0.044 V and 0.325 versus As the 5-HT concentration increased from 100–333 μM AA, the 5-HT current response increased, but 5-HT current response was higher than that of AA. However, as 5-HT concentration increased from 500–545 μM , the AA current response began to stabilize and drop while the 5-HT current response kept on increasing, as illustrated in figure 14(a). As the 5-HT concentration increased from 100–333 μM , the solution became saturated with 5-HT cationic molecules, resulting in a decrease in the AA peak current afterwards.

Furthermore, compared to anionic AA molecules, there was a better $\pi - \pi^*$ interaction between the f-MWCNTs and the cationic 5-HT molecules, resulting in better cationic 5-HT molecules attachment on the surface of the electrode. Figure 14(b) demonstrated that the 5-HT current peak increased linearly as concentration increased. Figure 15 depicts the simultaneous detection of 1 mM 5-HT and 1 mM AA at the modified electrode. The fabricated electrode exhibited excellent anti-interference behaviour even at fixed concentrations, as demonstrated by distinctive visible peaks of each analyte and a broad peak-to-peak separation of 367.90 mV between two analytes.



Stability, reproducibility, and shelve-life study

To analysis the effectiveness of the constructed electrochemical sensors, the stability, repeatability, and shelve studies were undertaken utilizing CV at a scan rate of 25 mVs^{-1} . The stability study was achieved by repeatedly scanning the electrode 20 times in 5 mM of $\text{K}[\text{Fe}(\text{CN})_6]^{3-/4-}$ made in 0.1 M PBS (pH 7). The repeated scans showed an increase in the anodic peak current of 26.39% and a decrease in the cathodic current peak by 17.71%, as shown in figure 16(a). An increase in anodic current peak could be ascribed to the increased electro-active interactions at the modified electrode's surface area with time. The results indicated that the constructed electrochemical sensor was not prone to biofouling during the voltammetry experiment and had excellent stability.

Similarly, the SPCE-MWCNT-AONP modified electrode was scanned repeatedly 20 times in 0.1 M PBS containing 0.1 mM 5-HT as an analytical probe. The anodic peak current of 5-HT decreased by 68% and demonstrated an RSD value of 34.42% towards 5-HT detection, as displayed in figure 16(b). The shelve-life study of the modified electrode was carried out every week in 0.1 mM 5-HT prepared in 0.1 M PBS (pH 7). The results of the experimentation are represented in figure 16(c). When the SPCE-MWCNT-AONP nanocomposite electrode was not in use, the electrode was kept in a dry environment. Figure 16(c) reveals that the current response decreased by 18% after 21 days, then increased by 1% after the 28 days, and then plummeted by 54% after the 35 days. The results confirm that the modified electrode has a long shelf life towards the detection of 5-HT.

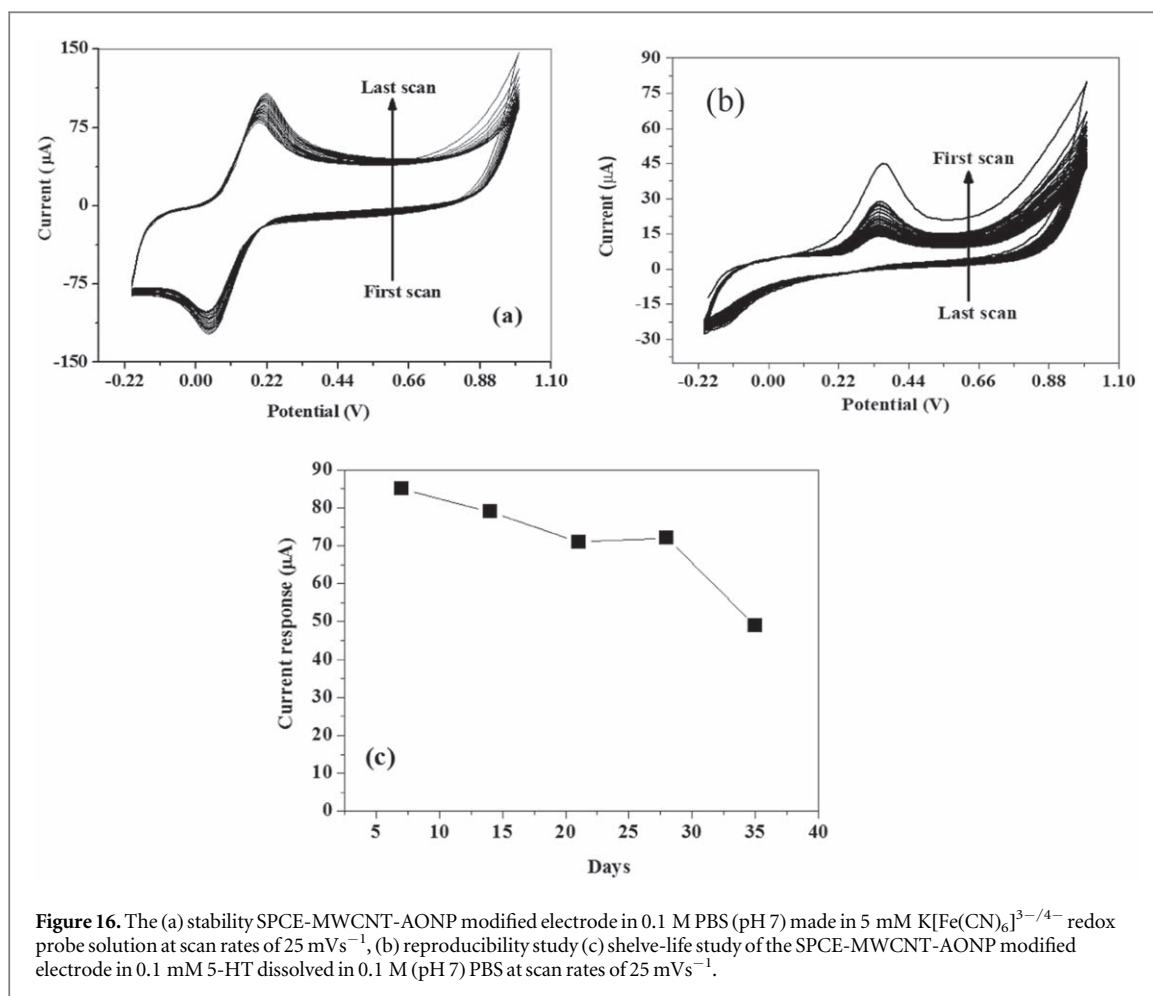


Figure 16. The (a) stability SPCE-MWCNT-AONP modified electrode in 0.1 M PBS (pH 7) made in 5 mM $K[Fe(CN)_6]^{3-/4-}$ redox probe solution at scan rates of 25 mVs^{-1} , (b) reproducibility study (c) shelf-life study of the SPCE-MWCNT-AONP modified electrode in 0.1 mM 5-HT dissolved in 0.1 M (pH 7) PBS at scan rates of 25 mVs^{-1} .

Table 3. Detection of 5-HT in tomato.

	Added (μM)	Detected (μM)	Recovery (%)	RSD (%)
Tomatoes	400	433.11	108.28	3.20
	600	547.92	91.32	2.60
	900	923.66	102.63	1.90

n = 3; mean RDS (%) = 2.57.

3.6. Real-sample analysis

The applicability of the fabricated sensor towards the determination of 5-HT in tomatoes was undertaken to utilize the SWV. The results from the experiment are summarized in table 3. For detection of 5HT in tomatoes, the SPCE-MWCNT-AONP modified electrode showed good recoveries ranging from 91.32%–108.28% with an average RSD (%) value of 2.57 (n = 3). This study suggests that the modified electrode is suitable for 5-HT detection in real samples.

4. Conclusion

In conclusion, electrochemical detection of 5-HT at the SPCE-MWCNT-AONP nanocomposite modified electrode has been achieved. The synthesized nanomaterials and nanocomposites were confirmed using FTIR; XRD, UV-vis, TEM, and SEM. Electrochemical studies were performed utilizing SWV and CV techniques. The SPCE-MWCNT-AONP nanocomposite modified electrodes showed excellent electron transport and better current response towards detection of 5-HT when compared to other electrodes studied. The reaction of 5-HT at SPCE-MWCNT-AONP nanocomposite modified electrode was diffusion controlled.

Moreover, the SPCE-MWCNT-AONP nanocomposite modified electrodes exhibited excellent selectivity and anti-interference capability towards detection of 5-HT in excess AA environment evidenced by the

observable peaks of each analyte and a wider peak-to-peak separation of 367.90 mV. A linear dependence of current response against 5-HT concentration was observed in the linear range of 0.016 μM –0.166 μM ($R^2 = 0.9851$) with sensitivity, LoD, and LoQ values of 0.2863 $\mu\text{A } \mu\text{M}^{-1}$, 0.025 μM , and 74 nM respectively. The proposed electrochemical sensor showed good reproducibility and long shelf life reaching half of its initial current response after 35 days. The proposed electrode was successfully tested towards detection of 5-HT in tomatoes with average recoveries of 100.74% and a mean RSD (%) value of 2.57 ($n = 3$). The proposed novel electrochemical sensor platform is of high interest for monitoring 5-HT and its therapeutic use.

Acknowledgments

The authors acknowledged the assistance of MASIIM of North-West University, NRF-Thutuka grant (UID 117709) and the Higher Degree of North-West University, Mafikeng Campus are also acknowledged.

Data availability statement

All data that support the findings of this study are included within the article (and any supplementary files).

Author contributions

OEF conceptualized and designed the work and was part of the manuscript write-up. PCM carried out the experiments, interpreted some of the results, and was also involved in the manuscript preparation. All the authors reviewed the manuscript and have agreed to its publication.

Conflicts of interest

Authors confirm that they have no conflict of interest.

ORCID iDs

Omolola E Fayemi  <https://orcid.org/0000-0002-0049-5184>

References

- [1] Yang L and Beal M F 2011 Determination of neurotransmitter levels in models of Parkinson's disease by HPLC-ECD methods *Mol. Biol.* **793** 401–15
- [2] Getinet A 2016 Common neurotransmitters; Criteria for neurotransmitters, key locations classifications and function *Adv. Psychol. Neurosci.* **1** 1–5
- [3] Tyng C M, Amin H U, Saad M N and Malik A S 2017 The influences of emotion on learning and memory *Front. Psychol.* **8** 1454
- [4] Walker M P and van der Helm E 2009 Overnight therapy ? The role of sleep in emotional brain processing *Psychol. Bull.* **135** 731–48
- [5] Hasanzadeh M, Shadjou N and Omidinia E 2013 A novel electro-analytical method for simultaneous detection of two neurotransmitters dopamine and serotonin in human serum *J. Neurosci. Methods* **219** 52–60
- [6] Tavakolian-Ardakani Z, Hosu O, Cristea C, Mazloun-Ardakani M and Marrazza G 2019 Latest trends in electrochemical sensors for neurotransmitters: a review *Sensors* **19** 2037
- [7] Campeau P M, Bernard G and Clayton P T 2007 Neurotransmitter diseases and related conditions *Mol. Genet. Metab.* **92** 189–97
- [8] Engbaek F and Voldby B 1982 Radioimmunoassay of serotonin (5-hydroxytryptamine) in cerebrospinal fluid, plasma, and serum *Clin. Chem.* **28** 624–8
- [9] Manbohi A and Ahmadi S H 2019 Sensitive and selective detection of dopamine using electrochemical microfluidic paper-based analytical nanosensor *Sen. Bio-Sens. Res.* **23** 100270
- [10] Cernat A, Ștefan G, Tertiș M, Cristea C and Simon I 2020 An overview of the detection of serotonin and dopamine with graphene-based sensors *Bioelectrochemistry.* **136** 107620
- [11] Hows M E, Lacroix L, Heidebreder C, Organ A J and Shah A J 2004 High-performance liquid chromatography/tandem mass spectrometric assay for the simultaneous measurement of dopamine, norepinephrine, 5-hydroxytryptamine and cocaine in biological samples *J. Neurosci. Methods* **138** 123–32
- [12] Yoshitake T, Kehr J, Todoroki K, Nohta H and Yamaguchi M 2006 Derivatization chemistries for determination of serotonin, norepinephrine and dopamine in brain microdialysis samples by liquid chromatography with fluorescence detection *Biomed. Chromatogr.* **20** 267–81
- [13] Zhang X, Fuller R R, Dahlgren R L, Potgieter K, Gillette R and Sweedler J V 2001 Neurotransmitter sampling and storage for capillary electrophoresis analysis *Fresenius J. Anal. Chem.* **369** 206–11
- [14] Aravind S J and Ramaprabhu S 2012 Dopamine biosensor with metal oxide nanoparticles decorated multi-walled carbon nanotubes *Nanosci. Methods.* **1** 102–14
- [15] Koyun O, Gorduk S, Arvas M B and Sahin Y 2018 Electrochemically treated pencil graphite electrodes prepared in one step for the electrochemical determination of paracetamol *Russ. J. Electrochem.* **54** 796–808

- [16] Khoshnevisan K, Honarvarfard E, Torabi F, Maleki H, Baharifar H, Faridbod F, Larijani B and Khorramizadeh M R 2020 Electrochemical detection of serotonin: a new approach *Clin. Chim. Acta* **501** 112–9
- [17] Habibi B, Jahanbakhshi M and Pournaghi-Azar M H 2011 Differential pulse voltammetric simultaneous determination of acetaminophen and ascorbic acid using single-walled carbon nanotube-modified carbon–ceramic electrode *Anal. Biochem.* **411** 167–75
- [18] Umeda S, Stagliano G W, Borenstein M R and Raffa R B 2005 A reverse-phase HPLC and fluorescence detection method for measurement of 5-hydroxytryptamine (serotonin) in Planaria *J. Pharmacol. Toxicol. Methods* **51** 73–6
- [19] Manjunatha J G, Swamy B K, Deraman M and Mamatha G P 2013 Simultaneous determination of ascorbic acid, dopamine and uric acid at poly (aniline blue) modified carbon paste electrode: A cyclic voltammetric study *Int. J. Pharm. Pharm. Sci.* **5** 355–62
- [20] Salimi A, Mamkhezri H and Hallaj R 2006 Simultaneous determination of ascorbic acid, uric acid and neurotransmitters with a carbon ceramic electrode prepared by sol–gel technique *Talanta* **70** 823–32
- [21] Xiao R, Beck O and Hjemsdahl P 1998 On the accurate measurement of serotonin in whole blood *Scandinavian J. Clin. Lab. Anal.* **58** 505–10
- [22] Alvarez J C, Bothua D, Collignon I, Advenier C and Spreux-Varoquaux O 1999 Simultaneous measurement of dopamine, serotonin, their metabolites and tryptophan in mouse brain homogenates by high-performance liquid chromatography with dual coulometric detection *Biomed. Chromatogr.* **13** 293–8
- [23] De Jong W H, Wilkens M H, De Vries E G and Kema I P 2010 Automated mass spectrometric analysis of urinary and plasma serotonin *Anal. Bioanal. Chem.* **396** 2609–16
- [24] Khoshnevisan K, Maleki H, Honarvarfard E, Baharifar H, Gholami M, Faridbod F, Larijani B, Majidi R F and Khorramizadeh M R 2019 Nanomaterial based electrochemical sensing of the biomarker serotonin: a comprehensive review *Microchim. Acta* **186** 49
- [25] Taleat Z, Khoshroo A and Mazloum-Ardakani M 2014 Screen-printed electrodes for biosensing: a review (2008–2013) *Microchim. Acta* **181** 865–91
- [26] Rodríguez-Méndez M L, Gay M, Apetrei C and De Saja J A 2009 Biogenic amines and fish freshness assessment using a multisensor system based on voltammetric electrodes. Comparison between CPE and screen-printed electrodes *Electrochim. Acta* **54** 7033–41
- [27] Wang J 1991 Modified electrodes for electrochemical sensors *Electroanalysis*. **3** 255–9
- [28] Aflatoonian M R, Tajik S, Aflatoonian B, Beitollahi H, Zhang K, Le Q V, Cha J H, Jang H W, Shokouhimehr M and Peng W 2020 A Screen-printed electrode modified with graphene/Co₃O₄ nanocomposite for electrochemical detection of tramadol *Front. Chem.* **8** 1065
- [29] Venugopal J and Ramakrishna S 2005 Applications of polymer nanofibers in biomedicine and biotechnology *Appl. Biochem. Biotechnol.* **125** 147–57
- [30] Chavali M S and Nikolova M P 2019 Metal oxide nanoparticles and their applications in nanotechnology *SN. Appl. Sci.* **1** 1–30
- [31] Falcaro P, Ricco R, Yazdi A, Imaz I, Furukawa S, Maspoch D, Ameloot R, Evans J D and Doonan C J 2016 Application of metal and metal oxide nanoparticles@ MOFs *Coord. Chem. Rev.* **307** 237–54
- [32] Nunes D, Pimentel A, Gonçalves A, Pereira S, Branquinho R, Barquinha P, Fortunato E and Martins R 2019 Metal oxide nanostructures for sensor applications *Semicond. Sci. Technol.* **34** 043001
- [33] Gao X, Zhou Q, Lu Z, Xu L, Zhang Q and Zeng W 2019 Synthesis of Cr₂O₃ nanoparticle-coated SnO₂ nanofibers and C₂H₂ sensing properties *Front. Mater.* **6** 163
- [34] Chang P R, Yu J and Ma X 2009 Fabrication and characterization of Sb₂O₃/carboxymethyl cellulose sodium and the properties of plasticized starch composite films *Macromol. Mater. Eng.* **294** 762–7
- [35] Karak N and Maiti S 1998 Antimony polymers. III. Flame retardant behaviour of chloroprene and natural rubber vulcanizates with antimony polymer *J. Appl. Polym. Sci.* **68** 927–35
- [36] Mostashari S and Baie S 2008 Thermogravimetry studies of cotton fabric's flame-retardancy by means of synergism of lithium bromide and antimony trioxide *J. Therm. Anal. Calorim.* **94** 97–101
- [37] Miura N, Mizuno H and Yamazoe N 1988 Humidity sensor using antimony phosphate operative at a medium temperature of 150–250°C *Jpn. J. Appl. Phys.* **27** 931
- [38] Badawy W A and El-Taher E A 1988 Preparation and electrochemical behaviour of some metal oxide films *Thin Solid Films* **158** 277–84
- [39] Sahoo N K and Apparao K V S R 1996 Process-parameter optimization of Sb₂O₃ films in the ultraviolet and visible region for interferometric applications *Appl. Phys. A* **63** 195–202
- [40] El-Diasty F, Abdel Wahab F A and Abdel-Baki M 2006 Optical band gap studies on lithium aluminium silicate glasses doped with Cr³⁺ ions *J. Appl. Phys.* **100** 093511
- [41] Tigau N, Ciupina V and Prodan G 2005 The effect of substrate temperature on the optical properties of polycrystalline Sb₂O₃ thin films *J. Cryst. Growth* **277** 529–35
- [42] Chin H S, Cheong K Y and Razak K A 2010 Review on oxides of antimony nanoparticles: synthesis, properties, and applications *J. Mater. Sci.* **45** 5993–6008
- [43] Zestos A G 2018 Carbon nanoelectrodes for the electrochemical detection of neurotransmitters *Int. J. Electrochem. Sci.* **2018** 1–19
- [44] Wang Z H, Liang Q L, Wang Y M and Luo G A 2003 Carbon nanotube-intercalated graphite electrodes for simultaneous determination of dopamine and serotonin in the presence of ascorbic acid *J. Electroanal. Chem.* **540** 129–34
- [45] McCreery R L 2008 Advanced carbon electrode materials for molecular electrochemistry *Chem. Rev.* **108** 2646–87
- [46] Fayemi O E, Adekunle A S and Ebenso E E 2015 Metal oxide nanoparticles/multi-walled carbon nanotube nanocomposite modified electrode for the detection of dopamine: comparative electrochemical study *J. Biosens. Bioelectron.* **6** 10–4172
- [47] Mphuthi N G, Adekunle A S, Fayemi O E, Olasunkanmi L O and Ebenso E E 2017 Phthalocyanine doped metal oxide nanoparticles on multi-walled carbon nanotubes platform for the detection of dopamine *Sci. Rep.* **7** 1–23
- [48] Fayemi O E, Adekunle A S and Ebenso E E 2017 Electrochemical determination of serotonin in urine samples based on metal oxide nanoparticles/MWCNT on modified glassy carbon electrode *Sens. Bio-Sens. Res.* **13** 17–27
- [49] Tsele T P, Adekunle A S, Fayemi O E and Ebenso E E 2017 Electrochemical detection of epinephrine using polyaniline nanocomposite films doped with TiO₂ and RuO₂ nanoparticles on multi-walled carbon nanotube *Electrochim. Acta* **243** 331–48
- [50] Saleh T A, Siddiqui M N and Al-Arfaj A A 2014 Synthesis of multi-walled carbon nanotubes-titania nanomaterial for desulfurization of model fuel *J. Nanomater.* **2014**
- [51] Li G, Xia Y, Tian Y, Wu Y, Liu J, He Q and Chen D 2019 Recent developments on graphene-based electrochemical sensors toward nitrite *J. Electrochem. Soc.* **166** B881
- [52] Le Hai T, Hung L C, Phuong T T B, Ha B T T, Nguyen B S, Hai T D and Nguyen V H 2020 Multiwall carbon nanotube modified by antimony oxide (Sb₂O₃/MWCNTs) paste electrode for the simultaneous electrochemical detection of cadmium and lead ions *Microchem. J.* **153** 10445653

- [53] Masibi K K, Fayemi O E, Adekunle S A, Sherif E S M and Ebenso E E 2018 Electrocatalysis of lindane using antimony oxide nanoparticles based-SWCNT/PANI nanocomposites *Front. Chem.* **6** 423
- [54] Çidem E, Tekler T and Aslanoglu M 2019 A sensitive determination of tramadol using a voltammetric platform based on antimony oxide nanoparticles *Microchem. J.* **147** 879–85
- [55] Zhou J, Sheng M, Jiang X, Wu G and Gao F 2013 Simultaneous determination of dopamine, serotonin and ascorbic acid at a glassy carbon electrode modified with carbon-spheres *Sensors* **13** 14029–40
- [56] Wang F, Wu Y, Lu K and Ye B 2013 A simple but highly sensitive and selective calixarene-based voltammetric sensor for serotonin *Electrochim. Acta* **87** 756–62
- [57] Uwaya G E and Fayemi O E 2020 Electrochemical detection of serotonin in banana at green mediated PPy/Fe₃O₄NPs nanocomposites modified electrodes *Sens. Bio-Sens. Res.* **28** 100338
- [58] Reddaiah K, Rao K S V K and Reddy T M 2018 Electrochemical detection of serotonin in human serum sample and simultaneous resolution in presence of epinephrine *Anal. Bioanal. Electrochem.* **10** 175–91
- [59] Lavanya N and Sekar C 2019 SnO₂-SnS₂ nanocomposite as electrocatalyst for simultaneous determination of depression biomarkers serotonin and tryptophan *J. Electroanal. Chem.* **840** 1–9
- [60] Chen X Y, Huh H S and Lee S W 2008 Hydrothermal synthesis of antimony oxychloride and oxide nanocrystals: Sb₄O₅Cl₂, Sb₈O₁₁Cl₂, and Sb₂O₃ *J. Solid State Chem.* **181** 2127–32
- [61] Ba Hashwan S S, Fatin M F, Ruslinda A R, Md Arshad M K, Hashim U and Ayub R M 2015 Functionalization of Multi-Wall Carbon Nanotubes Using Nitric Acid Oxidation *Appl. Mech. Mater.* **754** 1156–60
- [62] Jamal A, Rahman M M, Faisal M and Khan S B 2011 Studies on photocatalytic degradation of acridine orange and chloroform sensing using as-grown antimony oxide microstructures *Mater. Sci. Appl.* **2** 676
- [63] Jamal A, Raahman M M, Khan S B, Abdullah M M, Faisaal M, Asiri A M, Aslam A, Khan P and Akhtar K 2013 Simple growth and characterization of α-Sb₂O₄: Evaluation of their photo-catalytic and chemical sensing applications *J. Chem. Soc. Pak.* **35** 570
- [64] Jamal A, Rahman M M, Khan S B, Faisal M, Akhtar K, Rub M A, Asiri A M and Al-Youbi A O 2012 Cobalt doped antimony oxide nanoparticles based chemical sensor and photo-catalyst for environmental pollutants *Appl. Surf. Sci.* **261** 52–8
- [65] Zuber A, Purdey M, Schartner E, Forbes C, Van der Hoek B, Giles D, Abell A, Monro T and Ebdorff-Heidepriem H 2016 Detection of gold nanoparticles with different sizes using absorption and fluorescence based method *Sens. Actuators, B: Chem.* **227** 117–27
- [66] Obeid A, Al-Shuja' a O, El-Shekeil Y, Aqeel S, Salit M and Al-Washali Z 2018 New strategy for chemical attachment of Amide group on Multi-walled Carbon Nanotubes surfaces: synthesis, characterization and study of DC electrical conductivity *Curr. Chem. Lett.* **7** 17–26
- [67] Ahmed D S, Haider A J and Mohammad M R 2013 Comparison of functionalization of multi-walled carbon nanotubes treated by oil olive and nitric acid and their characterization *Energy Procedia* **36** 1111–8
- [68] Abuilwaihi F A, Laoui T, Al-Harhi M and Atieh M A 2010 Modification and functionalization of multi-walled carbon nanotube (MWCNT) via fischer esterification *Arab. J. Sci. Eng.* **35** 37–48
- [69] Cheraghali R 2011 Effect of dry & wet oxidation of multi-walled carbon nanotubes on their structures *Int. J. Acad. Res.* **3**
- [70] Buchholz B, Haspel H, Boldizsár T, Kukovec Á and Kónya Z 2017 pH-regulated antimony oxychloride nanoparticle formation on titanium oxide nanostructures: a photocatalytically active heterojunction *CrystEngComm* **19** 1408–16
- [71] Sharma S, Singh N, Tomar V and Chandra R 2018 A review on electrochemical detection of serotonin based on surface modified electrodes *Biosens. Bioelectron.* **107** 76–93
- [72] Mohd Bakhori N, Yusof N A, Abdullah J, Wasoh H, Ab Rahman S K and Abd Rahman S F 2020 Surface enhanced CdSe/ZnS QD/SiNP electrochemical immunosensor for the detection of *Mycobacterium tuberculosis* by combination of CFP10-ESAT6 for better diagnostic specificity *Mater.* **13** 149
- [73] Okpara E C and Fayemi O E 2019 Comparative study of spectroscopic and cyclic voltammetry properties of CuONPs from citrus peel extracts *Mater. Res. Express* **6** 105056
- [74] Laviron E 1979 General expression of the linear potential sweep voltammogram in the case of diffusionless electrochemical systems *J. Electroanal. Chem. Interf. Electrochem.* **101** 19–28
- [75] Fayemi O E, Adekunle A S and Ebenso E E 2015 Metal oxide nanoparticles/multi-walled carbon nanotube nanocomposite modified electrode for the detection of dopamine: comparative electrochemical study *J. Biosens. Bioelectron.* **6** 10–4172
- [76] Mazloum-Ardakani M and Khoshroo A 2014 High sensitive sensor based on functionalized carbon nanotube/ionic liquid nanocomposite for simultaneous determination of norepinephrine and serotonin *J. Electroanal. Chem.* **717** 17–23
- [77] Jin G P, Lin X Q and Gong J M 2004 Novel choline and acetylcholine modified glassy carbon electrodes for simultaneous determination of dopamine, serotonin and ascorbic acid *J. Electroanal. Chem.* **569** 135–42
- [78] Jacobs C B, Vickrey T L and Venton B J 2011 Functional groups modulate the sensitivity and electron transfer kinetics of neurochemicals at carbon nanotube modified microelectrodes *Analyst* **136** 3557–65